RECLAMATION
Managing Water in the West

Can SRH-2D replicate observed patterns of bedload tracer dispersion?

Research and Development Office
Science and Technology Program
Scoping Proposal Report
ST-2017-5049-01
Technical Report No. SRH-2017-36

U.S. Department of the Interior
Bureau of Reclamation
Research and Development Office

Sept. 2017

Mission Statements

Protecting America's Great Outdoors and Powering Our Future

The Department of the Interior protects and manages the Nation's natural resources and cultural heritage; provides scientific and other information about those resources; and honors its trust responsibilities or special commitments to American Indians, Alaska Natives, and affiliated island communities.

REPORT DOCUMENTATION PAGE		*Form Approved* *OMB No. 0704-0188*
T1. REPORT DATE: SEPT, 2017	**T2. REPORT TYPE:** RESEARCH	**T3. DATES COVERED** Oct. 1, 2015 – Sept. 30, 2017
T4. TITLE AND SUBTITLE Can SRH-2D replicate observed patterns of bedload tracer dispersion?		**5a. CONTRACT NUMBER** XXXR4524KS- RR4888FARD160090003 (8)
		5b. GRANT NUMBER
		5c. PROGRAM ELEMENT NUMBER 1541 (S&T)
6. AUTHOR(S) D. Nathan Bradley		**5d. PROJECT NUMBER** ST-2017-5049-01
		5e. TASK NUMBER
		5f. WORK UNIT NUMBER 86-68240
7. PERFORMING ORGANIZATION NAME(S) AND ADDRESS(ES) Sedimentation and River Hydraulics Group Technical Service Center, Bureau of Reclamation, Denver, CO 80225		**8. PERFORMING ORGANIZATION REPORT NUMBER**
9. SPONSORING / MONITORING AGENCY NAME(S) AND ADDRESS(ES) Research and Development Office U.S. Department of the Interior, Bureau of Reclamation, PO Box 25007, Denver CO 80225-0007		**10. SPONSOR/MONITOR'S ACRONYM(S)** **R&D:** Research and Development Office **BOR/USBR:** Bureau of Reclamation DOI: Department of the Interior
		11. SPONSOR/MONITOR'S REPORT NUMBER(S) ST-2017-5049-01
12. DISTRIBUTION / AVAILABILITY STATEMENT **Final report can be downloaded from Reclamation's website: https://www.usbr.gov/research/**		
13. SUPPLEMENTARY NOTES		
14. ABSTRACT *(Maximum 200 words)*		
15. SUBJECT TERMS SRH-2D, Hydraulic Modeling, River Simulation Frameworks		

16. SECURITY CLASSIFICATION OF:			**17. LIMITATION OF ABSTRACT** U	**18. NUMBER OF PAGES**	**19a. NAME OF RESPONSIBLE PERSON** D. Nathan Bradley
a. REPORT U	**b. ABSTRACT** U	**c. THIS PAGE** U			**19b. TELEPHONE NUMBER** 303-445-2565

S Standard Form 298 (Rev. 8/98)
P Prescribed by ANSI Std. 239-18

BUREAU OF RECLAMATION

Research and Development Office
Science and Technology Program

Sedimentation and River Hydraulics, Technical Service Center, 86-68240

Final Report ST-2017-5049-01
Technical Report SRH-2017-36

Title: Can SRH-2D replicate observed patterns of bedload tracer dispersion?

D. BRADLEY Digitally signed by D. BRADLEY Date: 2017.11.17 15:50:41 -07'00'

Prepared by: D. Nathan Bradley, Ph.D.
Physical Scientist, Sedimentation and River Hydraulics Group, TSC, 86-68240

Peer Review: David Gaeuman, Ph.D.
Physical Scientist, Trinity River Restoration Program

BUREAU OF RECLAMATION

Research and Development Office
Science and Technology Program

Sedimentation and River Hydraulics, Technical Service Center, 86-68240

Final Report ST-2017-FA105-01
Technical Report SRH-2017-36

Title: Can SRH-2D replicate observed patterns of bedload tracer dispersion?

D. BRADLEY Digitally signed by D. BRADLEY Date: 2017.11.16 12:51:45 -07'00'

Prepared by: D. Nathan Bradley, Ph.D.
Physical Scientist, Sedimentation and River Hydraulics Group, TSC, 86-68240

David Gaeuman

Peer Review: David Gaeuman, Ph.D.
Physical Scientist, Trinity River Restoration Program

Contents

Tables

Figures

Executive Summary

Gravel augmentation is a common strategy for improving fish habitat in rivers below dams. A dam blocks all sediment inputs from upstream, reducing the supply of transportable sediment downstream of the dam. Transportable sediment provides the substrate in which fish spawn and creates and maintains the diverse channel morphology that provides fish habitat (bars, pools, riffles). To compensate for the lack of transportable gravel below a dam, efforts to improve fish habitat often include adding gravel to the river. One example is the Trinity River in Northern California where Reclamation's Trinity River Restoration Project (TRRP) has added gravel below Lewiston Dam in hopes of improving habitat for anadromous Coho and Chinook salmon and steelhead. Despite the significant costs involved, predicting how introduced gravel will move and where it will be deposited is fraught with uncertainty. Gravel deposition in deep pools used as holding habitat and thermal refugia by adult fish and the blocking of access to juvenile rearing habitat in side channels are common unintended consequences of gravel augmentation that reduce, rather than increase, the amount of quality habitat. To avoid the unintended consequences of gravel augmentation, we need tools to predict the dispersion and fate of introduced gravel. Better computer simulation of the trajectory and fate of introduced gravel based on the channel morphology and flow hydraulics would make stream restoration projects that involve gravel augmentation more effective and less expensive. An accurate gravel dispersion model would guide decisions about the grain size distribution and quantity of augmented gravel as well as where and how it should be added to the river to best achieve the desired outcome.

In this report, I compare the sediment transport predictions of Reclamation's hydraulic and sediment transport model, SRH-2D (Sedimentation and River Hydraulics, Two-Dimensional), to a nine year sequence of gravel tracer transport observations from Halfmoon Creek, a gravel bed river near Leadville, CO. The positions of 893 rocks labeled with passive integrated transponder (PIT) tags were surveyed annually from 2007 to 2015 with recovery rates exceeding 90%. The PIT tags equip each tracer stone with a unique identifier that can be read from up to a meter away without disturbing the river bed. This large data set of gravel transport paths is compared to model predictions of sediment flux and topographic change.

I find that SRH-2D does not always conserve sediment mass. In spite of this significant limitation, there is remarkable correspondence between average model sediment flux and average tracer transport distance, both in the pattern and in the actual quantities. While the correspondence between yearly tracer concentration change and model topographic change is not as strong, the model is broadly consistent with the tracer results in that it predicts deposition on gravel bars and erosion in the stream segments between bars. Overall, the success of SRH-2D at predicting average tracer travel distance is surprising and suggests that SRH-2D could be useful in designing and analyzing gravel augmentation programs.

In addition to this report, this study resulted in a book chapter [*M. A. Hassan and Bradley*, 2017], a journal article submitted to Geophysical Research Letters that has been through three rounds of reviews [*Bradley*, In Review], and one that is being prepared [*Goodwin et al.*, In preparation].

Introduction

The sediment supply to a river downstream of a dam is reduced because sediment inputs from upstream are blocked. Without continuous replacement by upstream material, transportable sediment below a dam is winnowed away, resulting in a river bed that is coarser and less morphologically diverse. This negatively affects fish in at least two ways. First, river gravel of transportable size provides the substrate in which fish spawn. Second, mobile gravel creates and maintains the diverse channel morphology (bars, pools, riffles) that provides high quality aquatic habitat. Consequently, efforts to improve fish habitat below a dam commonly involve adding transportable sediment, typically gravel, to the river.

Unfortunately, predicting how introduced gravel will move and where it will be deposited involves significant uncertainty. Unintended deposition of gravel in pools or side channels reduces the amount of high quality habitat, increasing stream restoration costs and decreasing public confidence in restoration efforts. Accurate computer simulation of the dispersion and fate of introduced gravel would lower the cost and improve the effectiveness of stream restoration projects that involve gravel augmentation.

One common technique for observing bedload transport is to introduce “tracer” stones that are individually identifiable and can be tracked as they move downstream. Tracer clasts can be painted [e.g. *Laronne and Carson*, 1976], magnetically tagged [e.g. *Ferguson and Wathen*, 1998; *M.A. Hassan et al.*, 1991], equipped with active radio transmitters [e.g. *Ergenzinger and Schmidt*, 1990; *Schmidt and Ergenzinger*, 1992], or labeled with Passive Integrated Transponder (PIT) tags [e.g. *Allan et al.*, 2006; *Bradley and Tucker*, 2012; *Lamarre et al.*, 2005; *Liébault et al.*, 2012; *Nichols*, 2004]. This study used data from a large, extended tracer experiment to investigate the ability of a two dimensional hydraulic and sediment transport numerical model, SRH-2D [*Greimann et al.*, 2008; *Lai*, 2010], to reproduce the observed patterns of tracer gravel transport.

Halfmoon Creek Tracer Experiment

The tracer study is in an alluvial section of Halfmoon Creek, an alpine stream in the Sawatch Range of the Rocky Mountains near Leadville, CO USA (Figure 1). Halfmoon Creek is a snowmelt-driven stream that floods once a year during the spring or early summer. The drainage area at the upstream end of the study reach is about 61.5 km^2 and the elevation is 3,015 m. USGS stream gage (07083000) about 1.5 km downstream has been in operation since 1946. There are no tributaries between the study reach and the gage so it is assumed that the discharge at the study site is the same as that measured at the gage. The annual peak flood discharge averages 7.9 m^3/s [*U.S. Geological Survey*, 2013] and usually occurs in June. Summer thunderstorms are common, but do not produce much runoff [*Bradley and Tucker*, 2012; *Mueller and Pitlick*, 2005]. During the entire study period, the flow has exceeded 2 m^3/s outside of the spring snowmelt period only once. In August 2007, the flow reached 2.7 m^3/s, presumably as a result of a thunderstorm. This flow was well below the approximate tracer transport threshold of 3.5 m^3/s. Throughout the study area, the channel is approximately 10 m wide and about 1 m deep in the thalweg at bankfull discharge (~5.5 m^3/s). The bed slope averages 0.01. The median grain size along most of the reach is about 5.5 cm [*Bradley and Tucker*, 2012].

In May 2007, just before the spring flood, 893 gravel tracers labeled with Radio Frequency Identification (RFID) Passive Integrated Transponder (PIT) tags were installed on the bed of Halfmoon Creek in the area outlined in white in Figure 1, about 200 m upstream of a series of meanders and gravel bars. The PIT tags equip each rock with a unique identifier that can be read from a distance of up to ~0.5 m with little interference from water, sand, or gravel. PIT tags are increasingly popular for tracking bed load because they make it possible to identify a tracer without disturbing the stream bed and to recover a high percentage of the tagged rocks over an extended period of time [*Bradley and Tucker*, 2012; *Lamarre and Roy*, 2008; *Lamarre et al.*, 2005; *Liébault et al.*, 2012; *Nichols*, 2004; *Olinde and Johnson*, 2015; *Phillips and Jerolmack*, 2014; *Phillips et al.*, 2013; *Schneider et al.*, 2010].

The tracer population has a narrow grain size distribution (~80% in the range 4.8 – 6.7 cm) with a median b-axis diameter of 5.7 cm, similar to the D_{50} (median size) of the bed surface material, 5.5 cm. The tracer size distribution is shown in Figure 2. The stream was searched after each spring flood and the tracer positions were surveyed with a total station. Nine floods are analyzed here: 2007 to 2015. Figure 3 shows the USGS gage hydrographs for the study period. Tracer recovery rates have exceeded 90% in all years except 2013, when the detection equipment failed before the whole reach could be surveyed. The transport statistics and recovery rates are summarized in Table 1.

Table 1. The transport statistics and recovery rates for each flood year. The mean displacement and standard deviation is computed for mobile tracers only, defined as tracers that moved more than 1 m.

Year	Mean Displacement (m)	Standard Deviation (m)	Recovery Rate
2007	10.0	9.7	92.8%
2008	96.7	69.7	95.5%
2009	9.1	10.3	98.1%
2010	143.9	114.9	96.2%
2011	65.9	75.2	97.1%
2012	1.8	1.0	97.5%
2013	13.2	15.7	82.9%
2014	47.0	49.8	91.0%
2015	105.6	107.5	91.5%

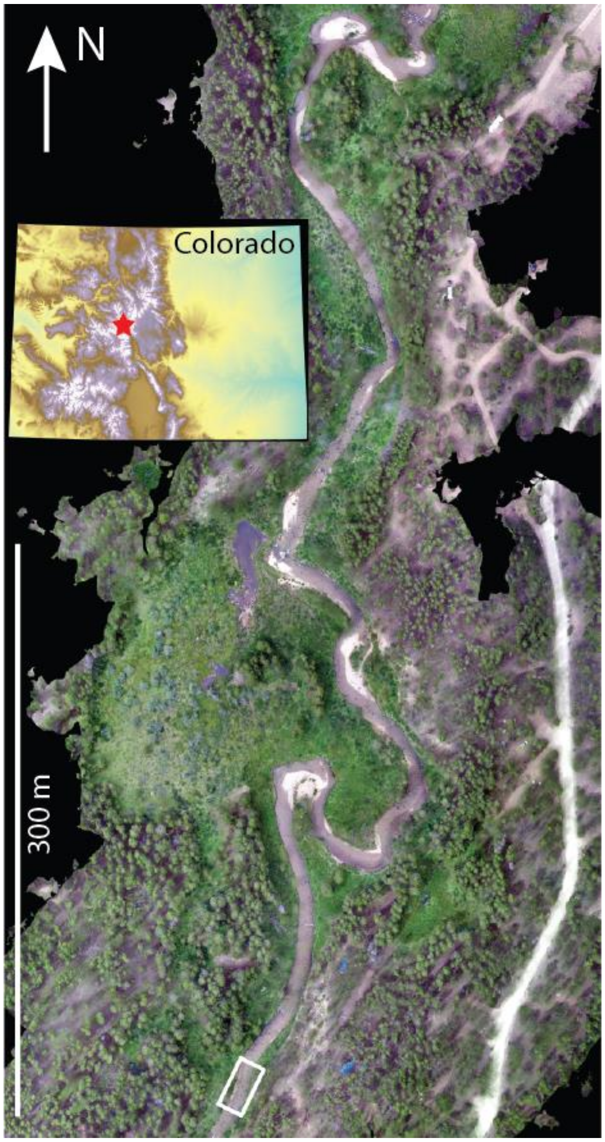

Figure 1. The Halfmoon Creek study area near Leadville, CO. The tracers were installed in May 2007 in the area outlined by the white rectangle.

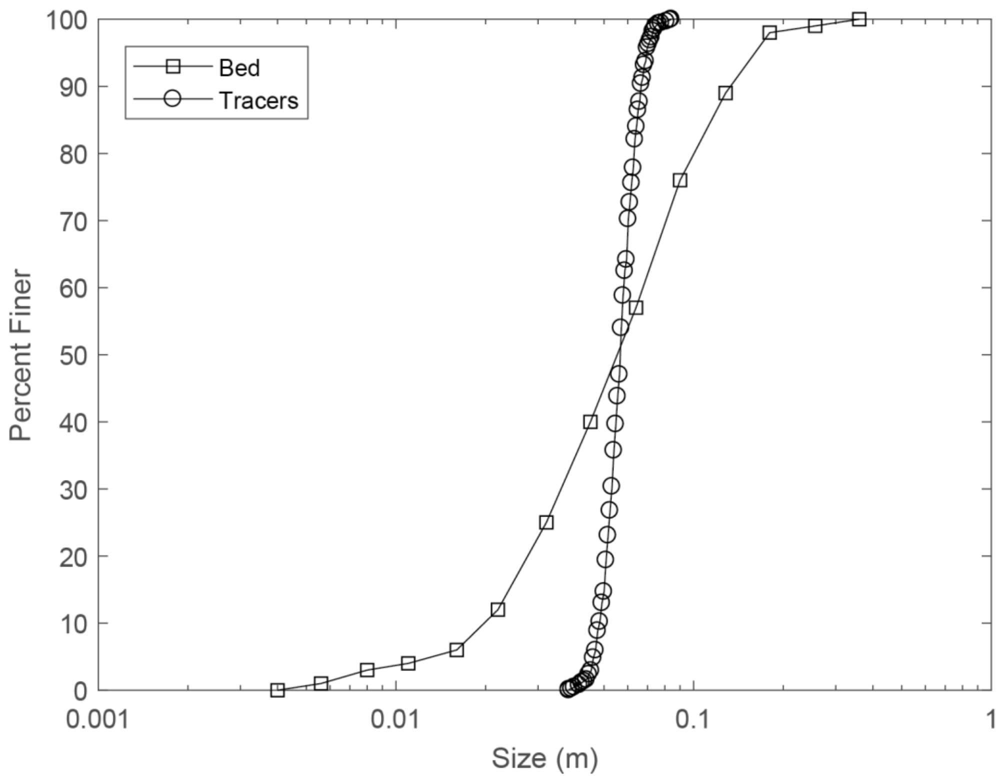

Figure 2. The tracer grain size distribution and bed surface size distribution.

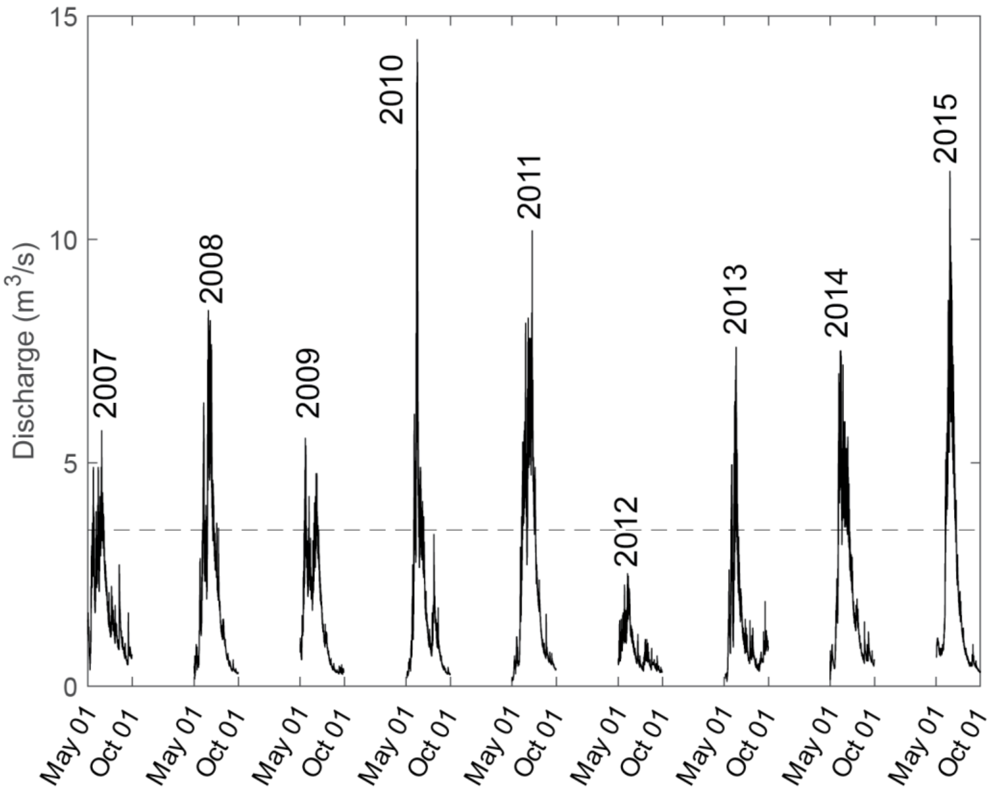

Figure 3. The hydrographs of the 9 floods studied here. The dashed line represents the approximate tracer transport threshold discharge, 3.5 m^3/s.

Model Development

The Sedimentation and River Hydraulics (SRH-2D) is a two dimensional numerical model that simulates the flow of water and sediment in a river. The data required for a river simulation with SRH-2D are 1) a representation of the topography of the river bottom and floodplain, 2) the grain size distribution of sediment on the bed of the river, 3) An inlet boundary condition of water and sediment fluxes, 4) an outlet boundary condition that specifies the relationship between flow and water surface elevation, and 5) observations of water surface elevation at a range of flows distributed along the study reach to calibrate the model.

The spatial data are then mapped onto a model mesh that discretizes the model domain so that the differential equations that describe the flow of water and sediment can be solved numerically. This section describes the development of the hydraulic and sediment transport SRH-2D simulations of Halfmoon Creek.

Topographic Survey and Terrain Development

In August 2015, a team from the USBR Sedimentation and River Hydraulics group, assisted by a professor and a graduate student from University of Cincinnati (Dr. Dylan Ward and Chris Sheehan), surveyed the Halfmoon Creek study reach with a Real Time Kinematic Global Positioning System (RTK GPS). We collected more than 5,000 GPS survey points over an area of approximately 18,400 m^2. After quality control, approximately 4,900 GPS points were used to create a topographic surface, for an average spatial resolution of about 3.7 m^2 per point. In the channel and on the banks immediately adjacent to the channel, the resolution is about 2.3 m^2 per point. This spatial resolution is consistent with our survey methodology of recording a point every meter along channel cross sections spaced about 2 m apart.

In addition to helping with the survey, Dr. Ward and his student used a small quad-copter to shoot aerial photography of the study reach. Dr. Ward then used Structure from Motion (SfM) to create a digital elevation model (DEM) of the study reach. The quad-copter footage was also used to create orthorectified images of the study reach, shown in Figure 1 and others.

After a quality control process, the GPS survey points were combined with breaklines generated from top of bank and bottom of bank survey points to create a triangular irregular network (TIN) of elevation. The survey points and breaklines are shown in Figure 4. The TIN was then combined with the SfM DEM generated by Dr. Ward to fill in the elevations of unsurveyed locations on the floodplain. Finally, a 3 m DEM from the USGS National Elevation Dataset (NED, https://nationalmap.gov/elevation.html) was used to fill in floodplain elevations in areas where the SfM DEM was affected by vegetation. The topographic surface used in the SRH-2D model is shown in Figure 5.

Dr. Ward and I explored the feasibility of using SfM generated topography for the SRH-2D model by comparing it to the GPS survey points. We found that on bare gravel bars and in shallow (< ~0.5 m), clear water, the GPS and SfM derived elevations were typically with +/- 5 cm of each other. However, SfM consistently underestimated the depth of the deeper pools (> 0.5 m). It is possible that multi-spectral methods could be used to correct for this effect, but we were not successful in our simple attempts to do so.

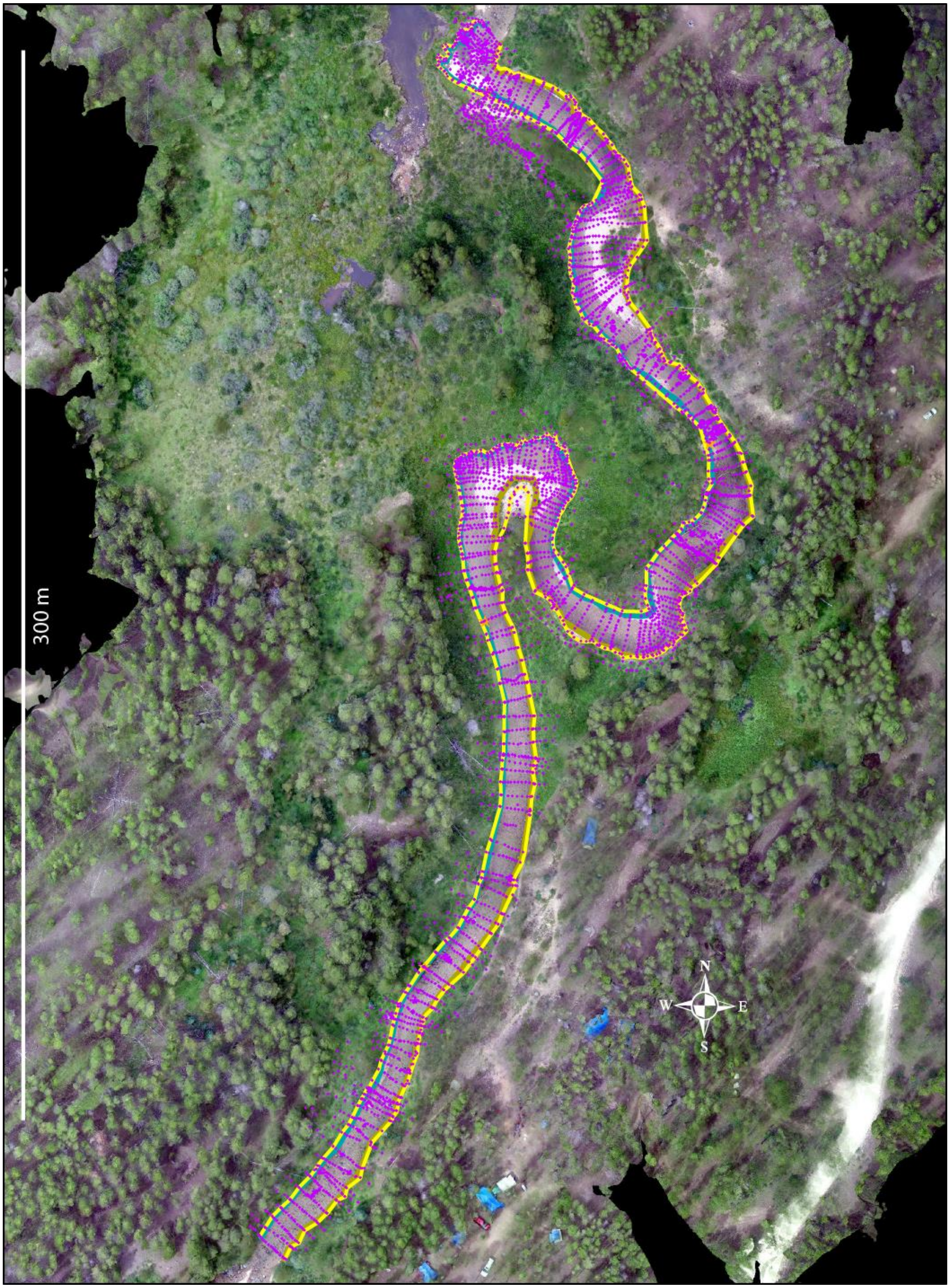

Figure 4. The GPS survey points (in pink) and the breaklines (yellow, top of bank; blue, bottom of bank) used to develop the topographic surface shown in Figure 5.

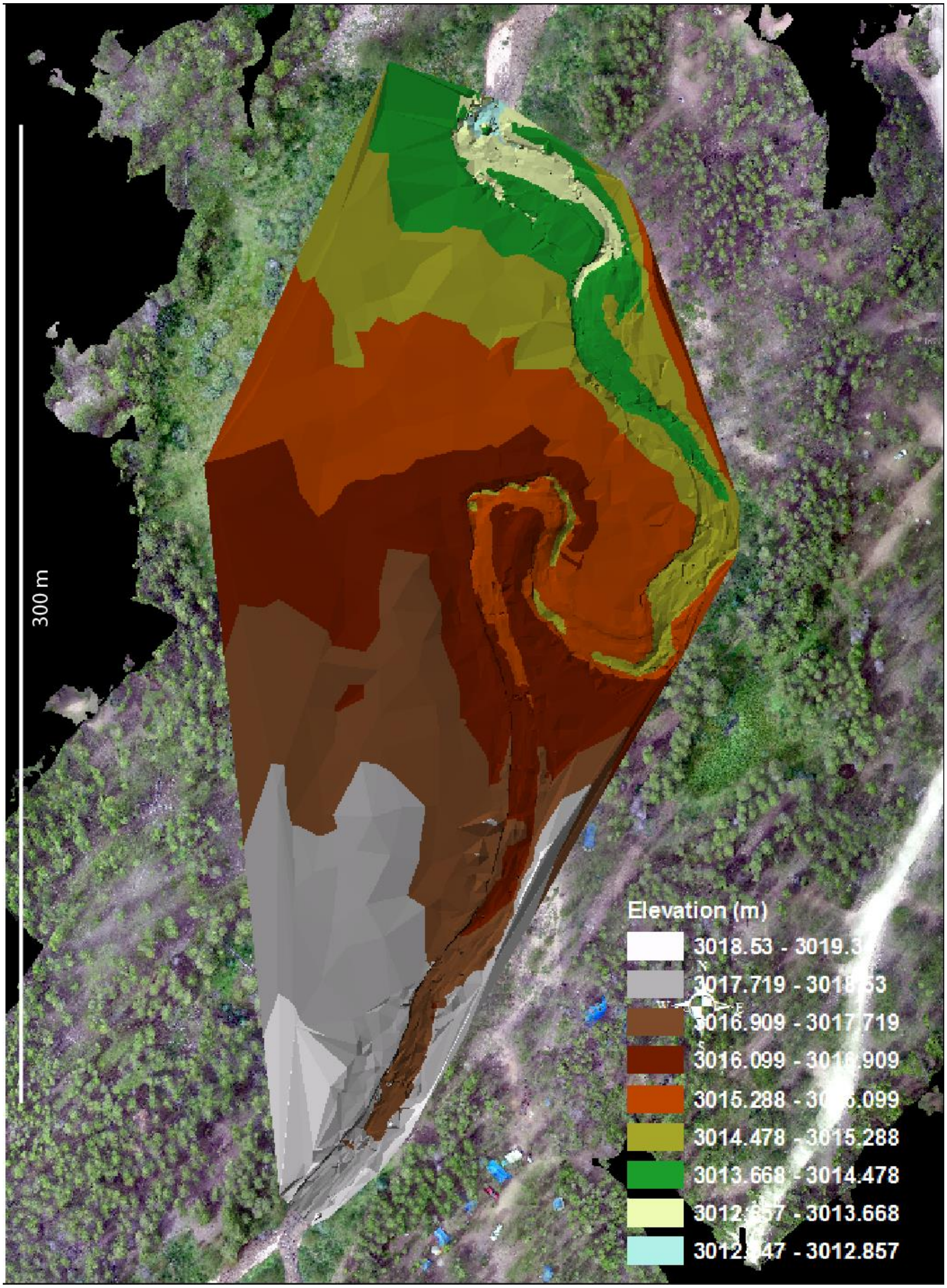

Figure 5. The topographic surface derived from the survey.

Water Surface Elevation Measurements

Observations of the water surface elevation at a range of flows are used to define the outlet boundary condition and to calibrate the hydraulic model. In the spring of 2015, I installed four ONSET U20L-04 HOBO [*ONSET*, 2017] pressure loggers along the length of the study reach to record water depth throughout the spring snowmelt flood (Figure 6). The loggers recorded water depth every 5 minutes from May 29 to Aug. 11, 2017. The water depths were converted to water surface elevations by adding the GPS surveyed elevation of the sensor to the measured depth. These water surface elevations were used to develop the outlet boundary condition and to calibrate the hydraulic model (described below).

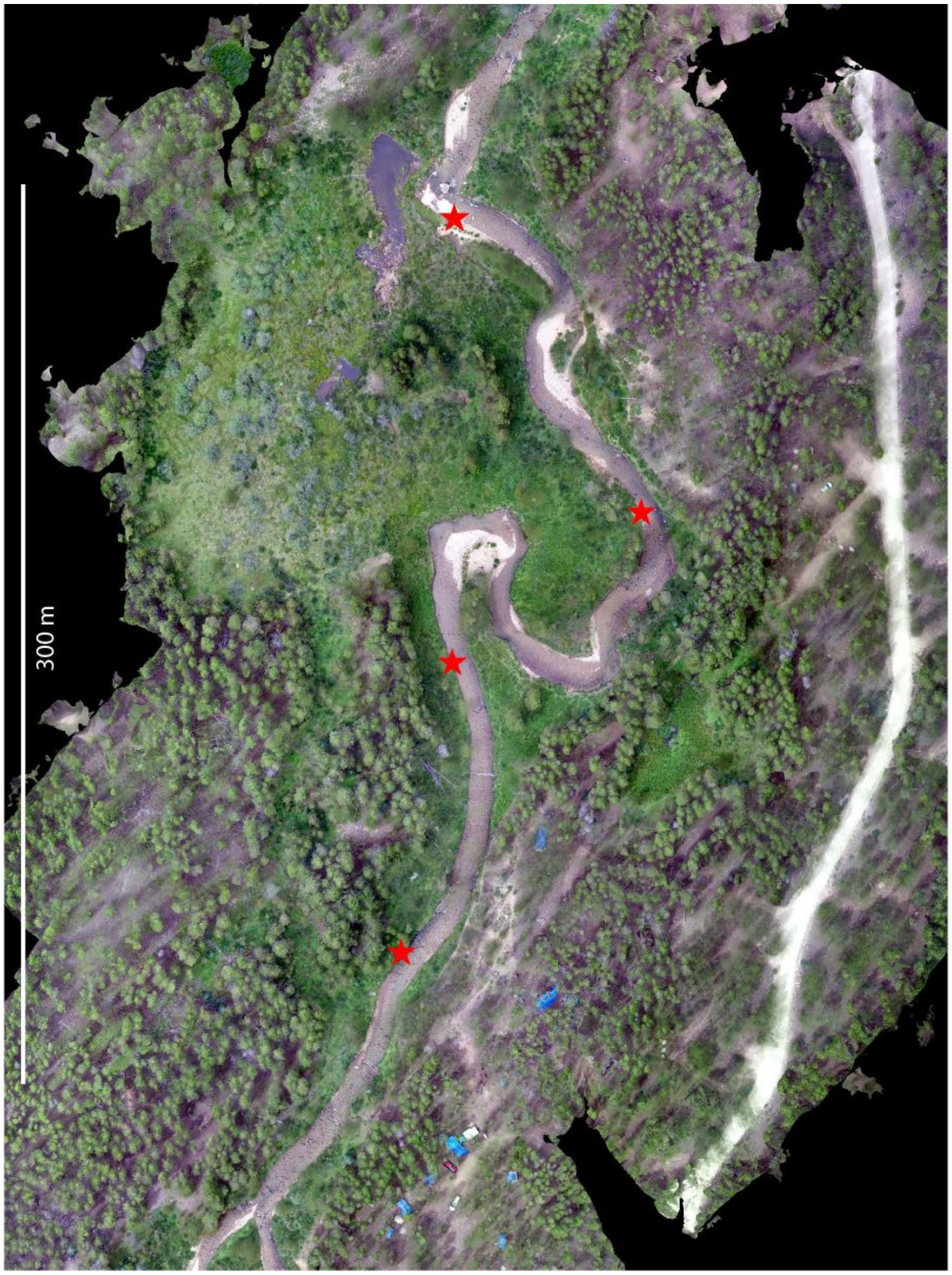

Figure 6. The locations of the HOBO pressure loggers deployed to record water depth during the 2015 spring flood.

Hydraulic Model

Before the sediment transport model could be developed, a hydraulics-only model was developed to calibrate the model water surface to the observed water surface elevations.

Mesh Development

The hydraulic model mesh was composed of rectangular elements in the channel and triangular elements on the floodplain for a total of 17,743 mesh elements. The channel elements are about 2 m long and about 0.5 m wide with an average area of about 0.8 m^2. The floodplain elements have an average area of about 5 m^2. The cumulative distributions of element size are shown in Figure 7.

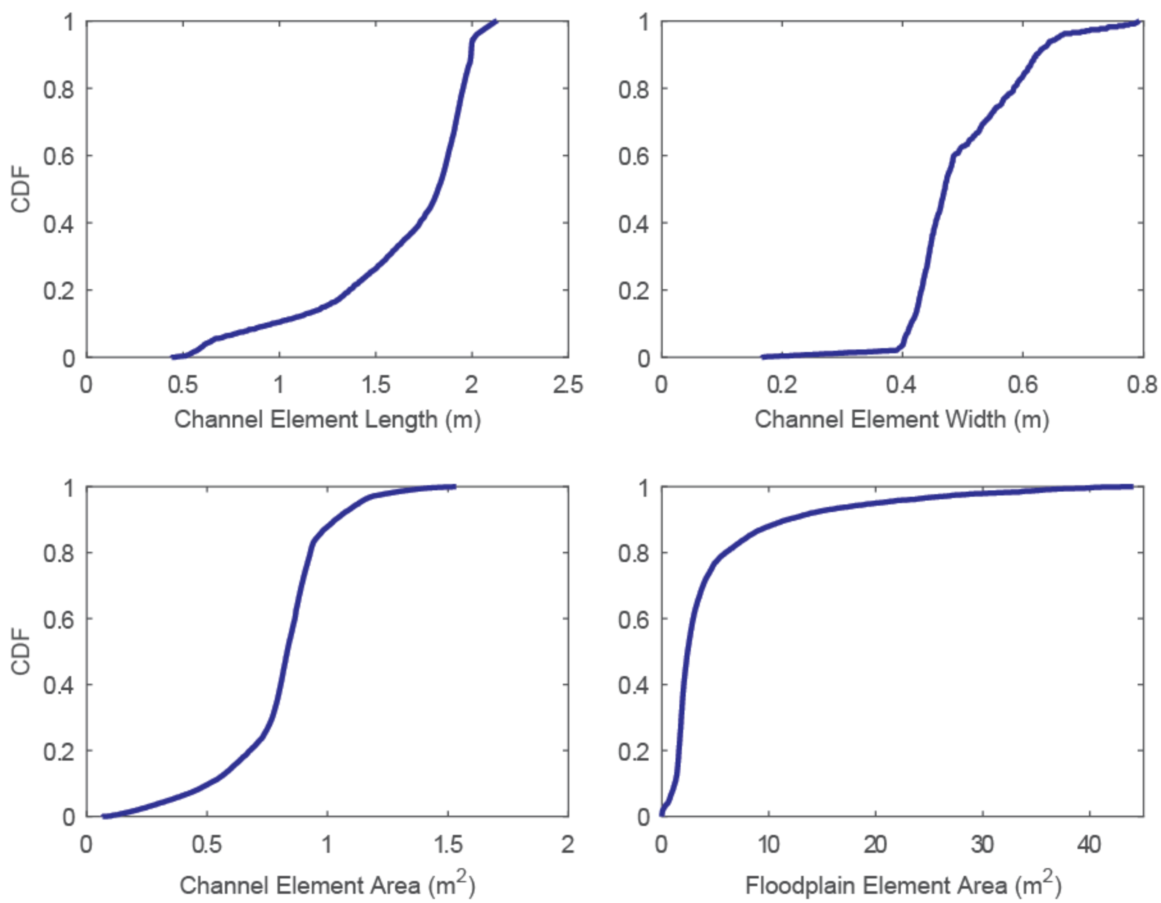

Figure 7. The distributions of the hydraulic model mesh element size and shape. Note that the x-axis changes scale in each plot.

Roughness

The main calibration parameter in SRH-2D is the flow resistance, parameterized as Mannings *n*. I assigned initial values of Mannings *n* to the mesh by dividing the channel into polygons of different estimated grain size and then computing Mannings *n* according to the following equation [*García*, 2008; *López and Barragán*, 2008]

$$n = \frac{C_m (2.8 D_{84})^{\frac{1}{6}}}{\left(8.1\sqrt{g}\right)}$$

where D_{84} is the 84th percentile of grain size in meters, g is the acceleration of gravity, and C_m is a coefficient equal to 1 for SI units. Overbank areas were assigned a roughness value of $n = 1$. The D_{84} for each roughness polygon is shown in Figure 8.

Boundary Conditions

Boundary conditions define how material (water, sediment) enters and exits the model domain. The upstream boundary condition of the hydraulic model is the inlet discharge time series taken from the USGS gage record and downsampled from 15 minutes to 1 hour intervals. The downstream boundary is a water surface elevation time series based on a discharge to water surface elevation relationship measured by the furthest downstream (northern most) HOBO pressure logger and projected downstream to the model boundary using the streamwise distance and the reach averaged water surface slope. A second order polynomial fit to this time series of water surface elevation vs. discharge served as a rating curve. This is shown in Figure 9. For a given discharge, there is about 5 cm of variation in the measured water surface elevation.

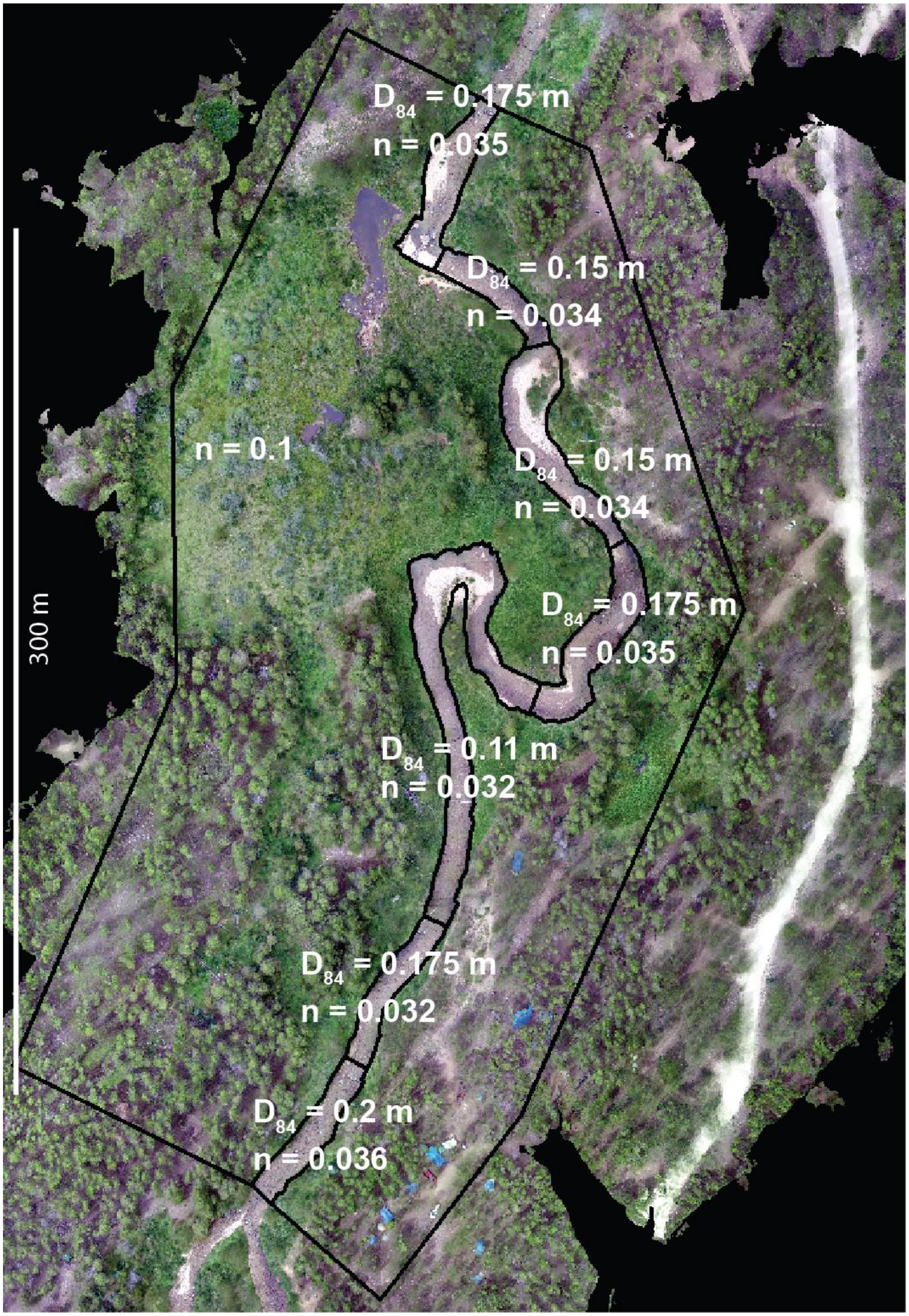

Figure 8. The grain size estimate used to assign initial values of Mannings n. The n-values shown are the final value after calibration and may be different from the initial values derived from the grain size estimate.

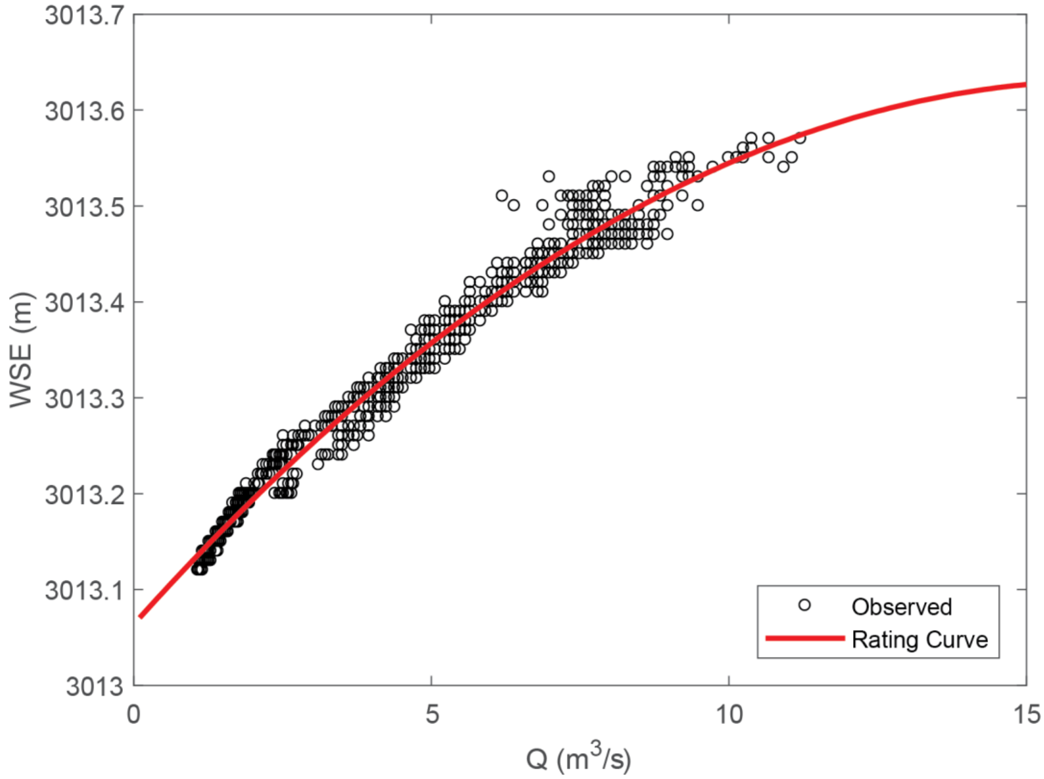

Figure 9. The 2nd order polynomial rating curve developed to set the downstream boundary condition. In general, there is about 5 cm of measured variation in water surface elevation for a given discharge.

Model Calibration

After the assignment of the initial values of Mannings n based on the estimate of the D_{84}, the model water surface elevation at SRH-2D monitoring points specified at the locations of the HOBO pressure loggers (see Figure 6) were compared to the observed water surface elevations. The roughness was then adjusted to improve the correspondence between the model and the observations. The final values of Mannings n are shown in Figure 8. The final calibrated water surface is within +/- 0.05 m at three of the four comparison locations (Figure 10). At one location (plotted in green in Figure 10) the modeled water surface is higher than the observed water surface elevation. I considered this misfit acceptable for two reasons. First, the pressure logger at this position registered negative water depths some of the time, suggesting that it may not be reliable. Second, the model water surface elevations correspond well to the observed water surface on some days, but not on others. For example, the green lines plotted in Figure 10 show a mismatch in the final week of June, but at a few days later, on about July 1, there is good correspondence at approximately the same flow. Tuning the roughness to match some days would likely cause a mismatch on others. Finally, field observations reveal flow in sub-surface channels underneath the floodplain that could be removing water from the channel in the vicinity of the first meander and returning it to the stream downstream of the pressure logger. The model cannot reproduce this effect.

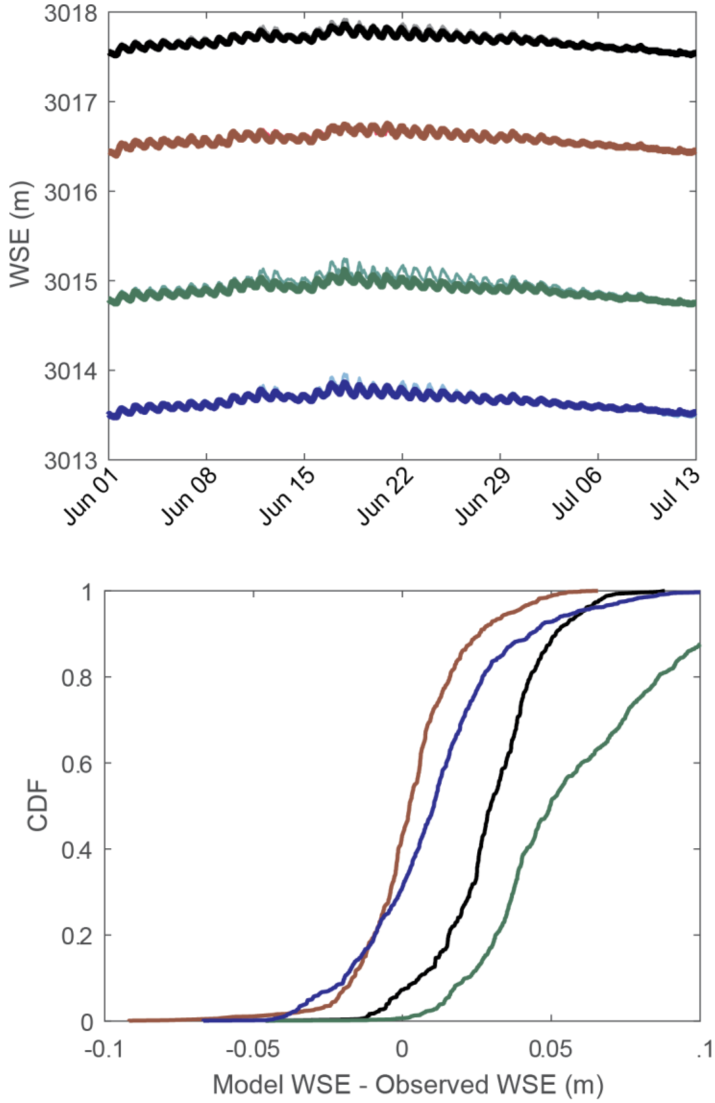

Figure 10. Top, the model water surface elevations (thin lines) compared to the water surface observations from the four pressure loggers over the course of the 2015 flood. Bottom, the cumulative distribution of the water surface elevation residuals indicate that the model is calibrated to the observations to within less than 5 cm at three of the four locations. The model water surface is 5-10 cm high at one of the locations, but that HOBO reported negative depths at various times, so it may not be reliable.

Sediment Transport Model

Extending the hydraulic model to a sediment transport model requires defining the bed characteristics (active layer thickness, number of layers, and the bed grain size gradation), the input boundary conditions (sediment fluxes by grain size class), designating any areas of cohesive or non-transportable material, and choosing a sediment transport capacity equation.

I chose to develop as simple a model as possible. I divided the model domain into a transportable channel zone and a cohesive, non-transportable floodplain zone. In the channel zone, I specified a two-layer model with identical grain size distributions and an active layer that is 0.25 m thick, approximately two times the surface D_{90} [*DeVries*, 2002; *Judith K Haschenburger and Church*, 1998; *M. A. Hassan and Bradley*, 2017; *Wilcock and McArdell*, 1997; *Wilcock et al.*, 1996]. I used the Wilcock capacity equation which is appropriate for mixed sized sediment in the gravel and cobble size class [*Wilcock and Crowe*, 2003]. The adaptation length formulation of *Seminara et al.* [2002] was used.

Grain size data

The grain size data used in the model are surface grain size distributions collected by *Mueller and Pitlick* [2005] and shared courtesy of Erich Mueller (Table 2, Figure 3). I assume that the grain size distribution of the stream bed has been steady over the course of the study. Qualitative observations since 2007 support the assumption that the sediment grain size is at least quasi-steady. The grain size distribution shown in Figure 3 was discretized into 13 size classes, shown in Table 2. These size gradations were specified for both layers of the two layer model. The top layer was 0.25 m thick and the bottom layer was 5 m thick.

Table 2. The grain size distribution used in the SRH-2D sediment transport model.

Size class minimum (mm)	Size class maximum (mm)	Percent finer
4	5.6	0%
5.6	8	1%
8	11	3%
11	16	4%
16	22	6%
22	32	12%
32	45	25%
45	64	40%
64	90	57%
90	128	76%
128	180	89%
180	256	98%
256	360	99%
360+		100%

Inlet Sediment Flux Boundary Condition

There are at least two options for specifying the upstream sediment supply boundary condition in an unsteady SRH-2D simulation: 1) Specify a time series of sediment flux for each grain size class, or 2) Specify a rating curve that defines the sediment flux for each grain size class at a range of water discharges. I chose the second option.

Mueller and Pitlick [2005] estimated that the annual sediment flux in Halfmoon Creek is on the order of 10 m^3/year based on the amount of sediment in a retention basin about 3 km downstream of the study reach that is cleaned out each year. I consider this to be a very rough estimate of the actual sediment flux in the study reach, so I developed a sediment rating curve with the goal of minimizing topographic change throughout the study reach. From year to year, I have observed local scour and deposition of up to approximately 0.5 m, mostly around the tight meander bends, but overall, the reach is more or less in topographic equilibrium, defined as a divergence of sediment flux that is approximately zero over the study reach.

I used an iterative, trial and error method to develop the rating curve. I created transport-limited model with an oversupply of input sediment and bed sediment and created empirical rating curves for each grain size class from the outlet sediment flux. These rating curves were then used as the input to the actual model of the study reach. The sediment supply to the transport limited model was adjusted and the output flux scaled (by some multiplier) until I found rating curves that yielded minimal topographic change and similar input and output sediment fluxes in subsequent model runs. This was complicated by the fact that SRH-2D does not perfectly conserve sediment mass (see below), but the process eventually yielded an input boundary sediment rating curve that did not cause unrealistic erosion or deposition.

The transport-limited model used a simplified, triangular hydrograph with water discharge that started at 1 m^3/s, increased linearly by 0.1 m^3/s each hour to peak at 15 m^3/s, and then declined linearly back to 1 m^3/s. The model had a total substrate thickness of 5 m, which insured that bed sediment was readily available. The outlet sediment flux time series, shown in Figure 11, is noisy, with sudden spikes in sediment flux of many orders of magnitude. The meaning of these spikes in sediment is unclear. It is possible that they represent packets of sediment eroded from upstream suddenly crossing the outlet monitoring line. Some of the transport spikes occur simultaneously across multiple grain size classes (e.g. around 100 hours), which would support this idea. However, some spikes occur in only one grain size class (e.g. 180 mm at about 190 hours). Sediment transport is widely acknowledged to be an intermittent, stochastic process [e.g. *Bradley et al.*, 2010], however the sediment transport capacity approach used by SRH-2D seems unlikely to capture this stochasticity when the model flow varies slowly and ample sediment is for transport. This issue deserves further investigation.

To create a rating curve, the outlet sediment and water flux time series were sorted by increasing water flux and the sediment flux for each grain size class was plotted against water flux (Figure 12a). As expected, the resulting plots are noisy, with spikes in sediment flux for a given discharge of many orders of magnitude (the model flowed at each water discharge for 1 hour).

To smooth the rating curves (and investigate the source of the noise), I binned the raw sediment flux rating curves into 0.2 m^3/s bins of water discharge and examined the statistics (mean, median, mode, minimum) of the sediment flux values in each bin. I found that the minimum value of sediment flux (for each grain size class) in each bin was essentially identical to the modal value, suggesting that there is something anomalous about the spikes in sediment discharge that is not representative of the "actual" flux, which is better represented by minimum and model values. The bin-minimum curves are much smoother than the raw curves and even show transport thresholds for gravel and cobble grain size classes (Figure 11b). I chose to use these curves in the model.

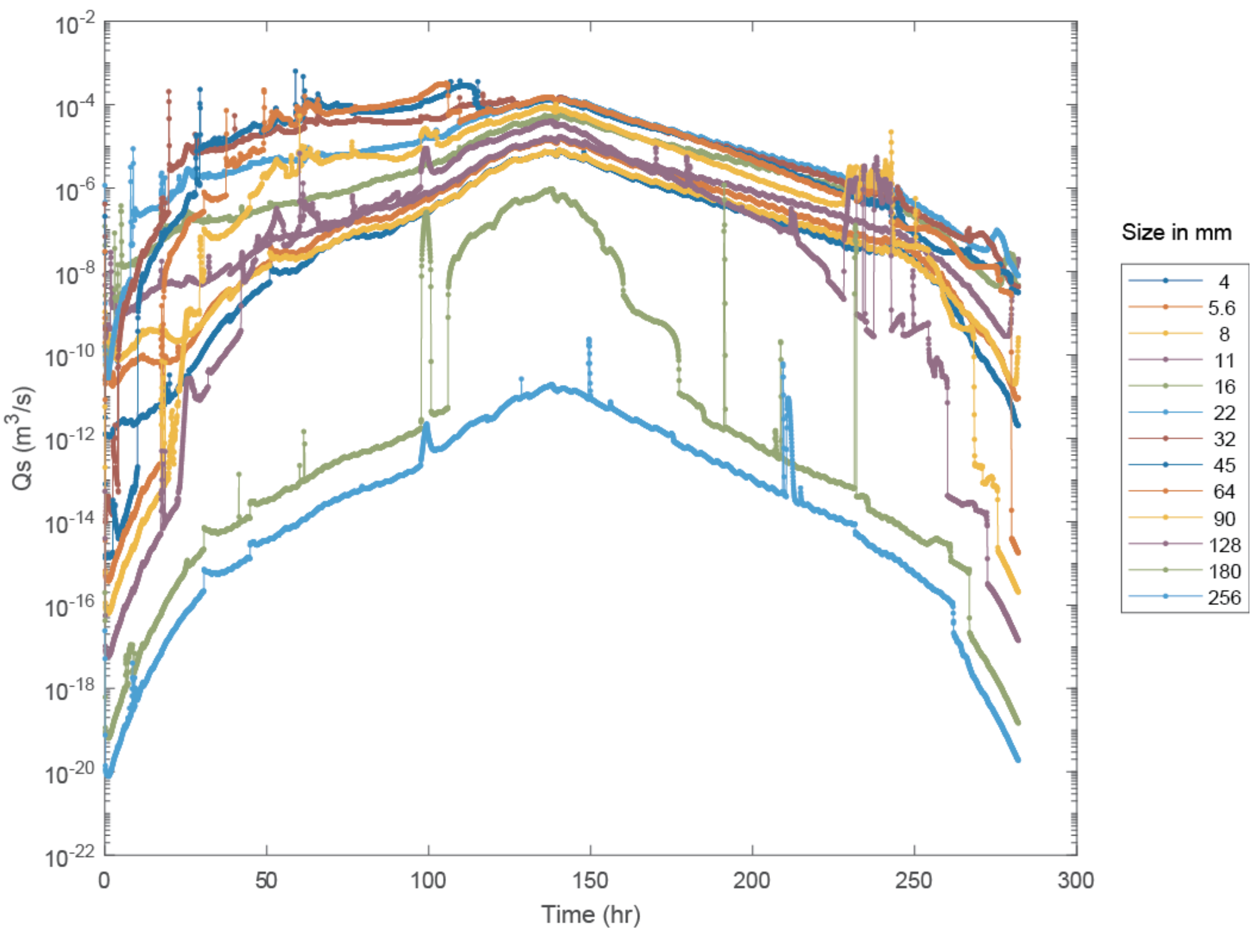

Figure 11. The outlet sediment flux time series for each grainsize class derived from the outlet monitoring line. The time resolution of the plot is 200 seconds.

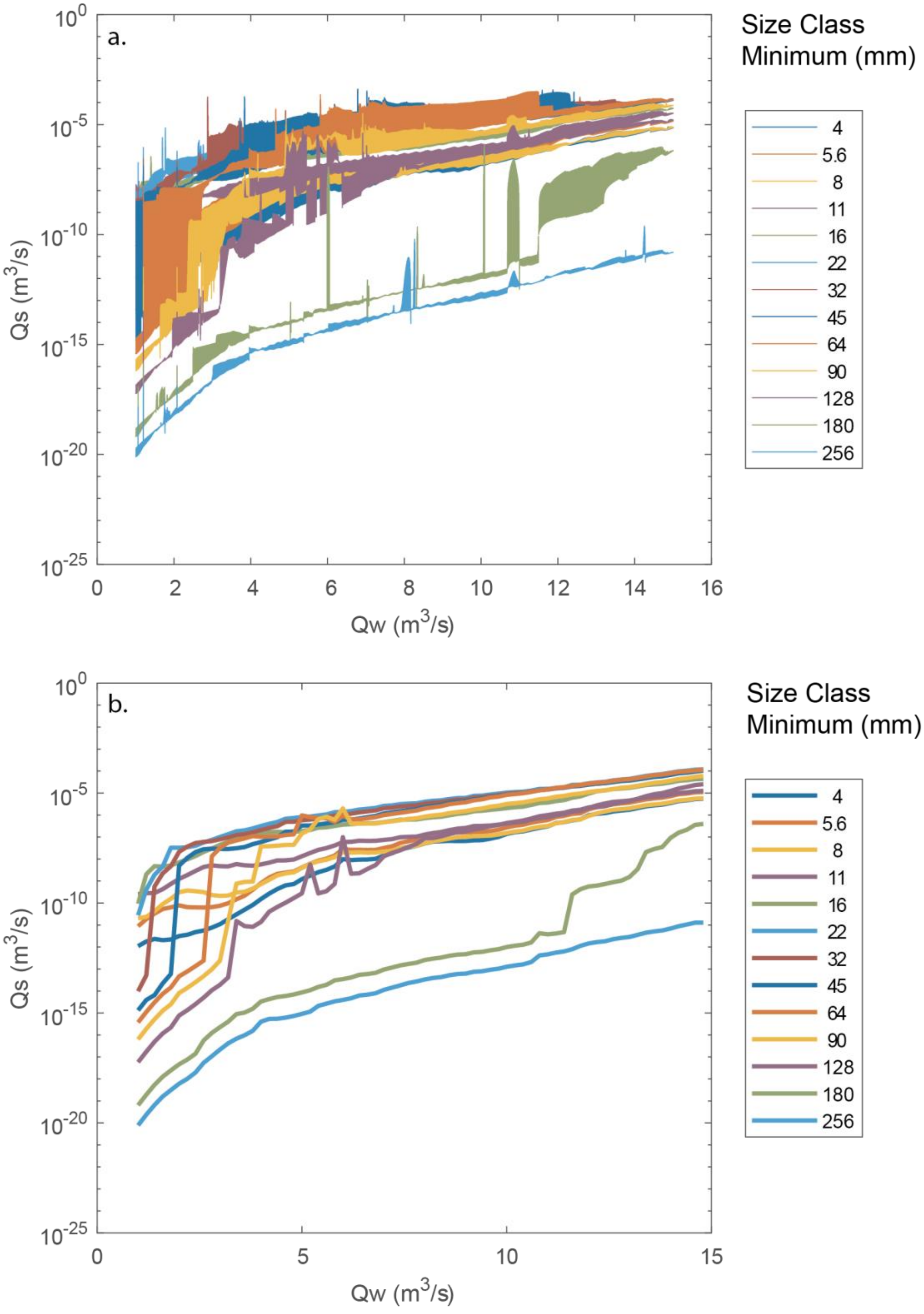

Figure 12. The sediment rating curve was developed from the output flux of a transport limited, simplified model. a) The raw sediment flux to water flux. b) The modal (minimum) value of sediment fluxes at each water discharge.

Model Runs

The SRH-2D simulation was run for the period of May 1 to Sept. 30 (2,208 model hours) for each of the nine flood hydrographs shown in Figure 3. Most flood simulations used a time step of 5 seconds, though two simulations required a shorter time steps to prevent model divergence. Experiments during the model development phase showed that noise in the sediment flux time series and issues with conservation of sediment mass were mostly insensitive to a reduction in time step size from 5 seconds to 1 second.

Analysis Methods

Conservation of Model Sediment Mass

To analyze sediment and water transport through the model, I divided the model domain using monitoring lines that correspond approximately to changes in the morphology of the stream (Figure 13). SRH-2D logs the sediment flux through the model inlet, model outlet, and monitoring lines to output files at regular output intervals. The output interval is based on the time step size and for the model runs analyzed here was typically less than 10 minutes of model time. These sediment flux data were integrated over time to yield a change in sediment storage volume that can be compared to the amount of sediment eroded from or deposited on the bed.

The total sediment volume transported across a monitoring line or model boundary, V_s, is obtained by trapezoidal integration of the sediment flux

Equation 1

$$V_s = \sum_{i=1}^{T} \frac{\left(Q_{s_i} + Q_{s_{i-1}}\right)}{2} (t_i - t_{i-1})$$

where Q_{s_i} is the volumetric sediment transport rate across the line during the i^{th} interval, t_i is the output time and T is the total number of time steps in the model run.

The total sediment derived from the model streambed surface over a model run $V_{s_{bed}}$ is

Equation 2

$$V_{s_{bed}} = (1 - p) \sum_{j=1}^{N} -\Delta z_j A_j$$

where p is the bed sediment porosity (set to 0.4), $-\Delta z_j$ is the total erosion depth of the j^{th} cell reported by the model, A_j is the cell area, and the summation is over the number of model cells,

$N.V_{s_{bed}}$ is positive if there is net erosion of the stream bed (contributing sediment to the flux) and negative if there is net deposition (sediment is lost from the flux).

Mass conservation for the entire model run is

Equation 3

$$V_{s_{inlet}} + V_{s_{bed}} = V_{s_{outlet}} + V_{s_{transport}}$$

Where $V_{s_{transport}}$ is the volume of sediment still in transport at the end of the model run. This volume is typically small relative to the other terms in the equation, but it is given by

Equation 4

$$V_{s_{transport}} = \sum_{j=1}^{N} \frac{10^{-6} C_j}{\left(\gamma + \left(10^{-6}(1-\gamma)C_j\right)\right)} A_j\, h_j$$

Where C_j is the concentration of entrained sediment in the j^{th} cell in parts per million of water, h_j is the water depth in the cell, γ is the specific gravity of sediment (set to 2.65), and the summation is over all the cells in the model.

The model's conservation of mass can be analyzed in more detail by comparing the fluxes of sediment transported across two adjacent monitoring lines with the bed elevation change integrated over the polygon formed by the channel banks and the monitoring lines (Figure 12). Adapting the conservation of mass equation for two adjacent monitoring lines and rearranging so that the left side is analogous to a divergence of flux gives

Equation 5

$$V_{s_k} - V_{s_{k-1}} = -V_{s_{bed_k}} + V_{s_{transport_k}}$$

Where k is used as both the index of the monitoring line (at the model inlet, $k = 0$) and as the index of the polygon upstream of the k^{th} monitoring line. The terms on the right hand side of the equation are calculated in the same way as in Equation 2 and Equation 4 except that the summation is only over the cells within the k^{th} polygon.

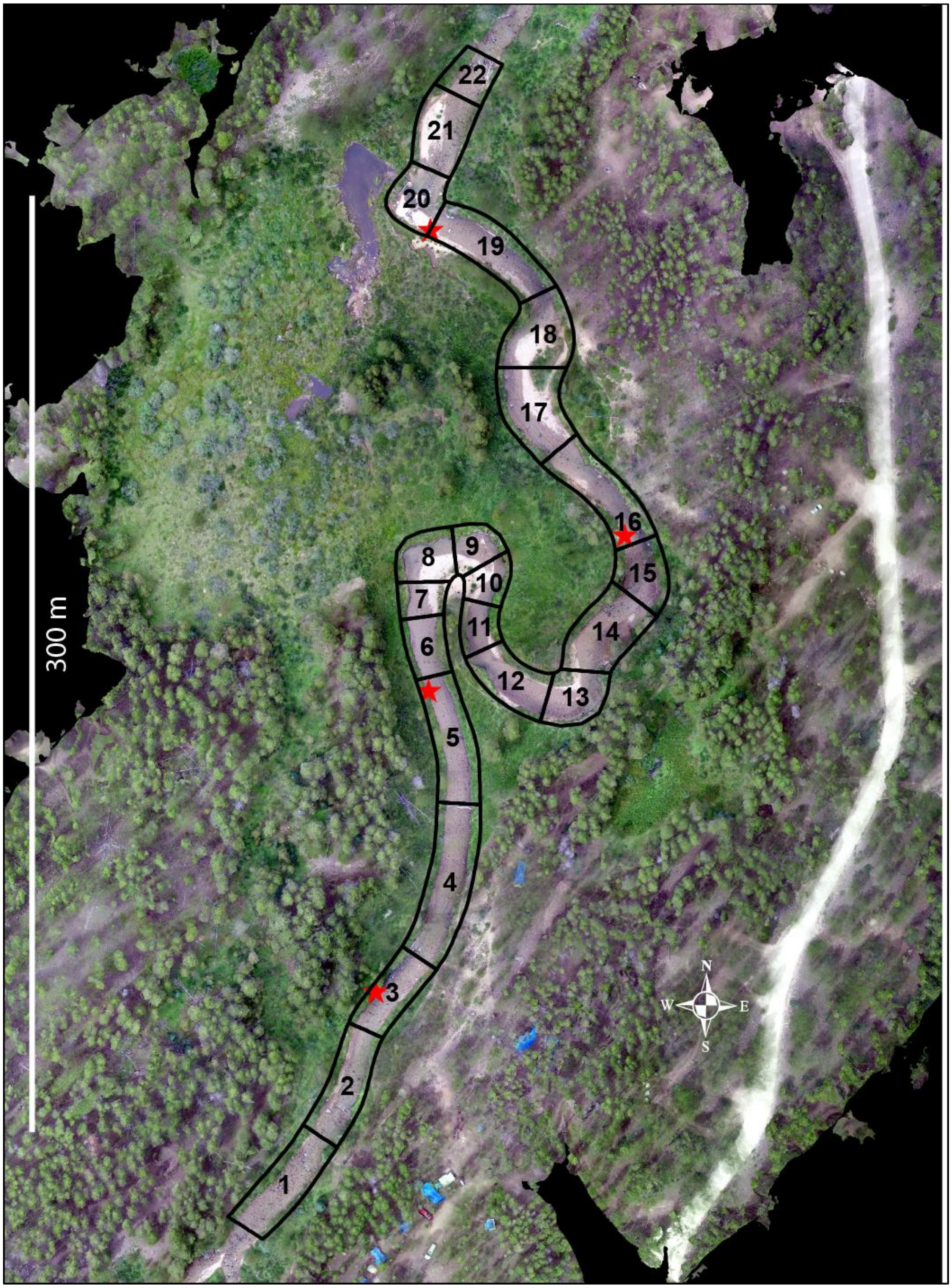

Figure 13. The monitoring lines and polygons used in the analysis of conservation of mass. The tracers were installed in the area outlined by the white rectangle in May 2007. The red stars mark the locations of the stage sensors used in model calibration.

Comparing Model Sediment Flux to Tracer Travel Distance

Mean Tracer Travel Distance vs. Cumulative Excess Energy

Cumulative Excess Energy

In this section, I examine tracer diffusion as a function of the cumulative excess energy. Cumulative excess energy is time-integrated excess stream power. It is conceptually similar to cumulative dimensionless impulse in that it is a time-integrated hydraulic forcing, but it does not require the spatial averaging of water depth used by the dimensionless impulse approach. The approach is nearly identical to that of *J Haschenburger* [2011b], with the addition of a transport threshold. Stream power $\Omega = \rho g Q S$ is the rate at which a stream dissipates energy against the bed and banks per unit length (in watts/m), where ρ is the density of water, Q is the volumetric water discharge, and S is the bed slope [*Bagnold*, 1977]. The cumulative excess energy E_t (joules/m) is the amount of energy expended above a transport threshold over a flood of duration $T = t_f - t_s$

Equation 6

$$E_t = \int_{t_s}^{t_f} (\Omega - \Omega_c) dt\,, \qquad \Omega > \Omega_c$$

where the threshold stream power $\Omega_c = \rho g Q_c S$ is the stream power at a threshold discharge. Exceedance plots of excess stream power for each year are shown in Figure 14. Cumulative excess energy for each flood (2007-2015) for the period between May 1 (t_s) and Sept. 30 (t_f) was computed according to Equation 6 with $\rho = 1000\ m^3/s\,, g = 9.81\ m/s^2$, $S = 0.01$, and Q equal to the average discharge at the gage over each measurement interval. The threshold discharge $Q_c = 3.5\ m^3/s$ corresponds to a Shields stress of approximately 0.035 for the D_{50} of the tracer population in the upstream part of the study reach. This value is somewhat lower than that predicted by the relationship developed by *Mueller et al.* [2005] for high gradient gravel and cobble bed streams (0.043), but it is consistent with observations of the stream bed during tracer installation (at flows between 2.2 and 3.2 m^3/s) and it is retained for consistency with *Bradley and Tucker* [2012]**.** Figure 14 shows the exceedance probabilities of excess stream power computed from the stream gage discharge record at 15 minute intervals for each year. The energy expenditure was calculated over all possible intervals between May 2007 and the end of the 2015 flood. The cumulative excess energy from year i to year j is

Equation 7

$$E_{ij} = \sum_{y=i}^{y=j} E_y$$

where E_y is the total excess energy expended in year i through year j.

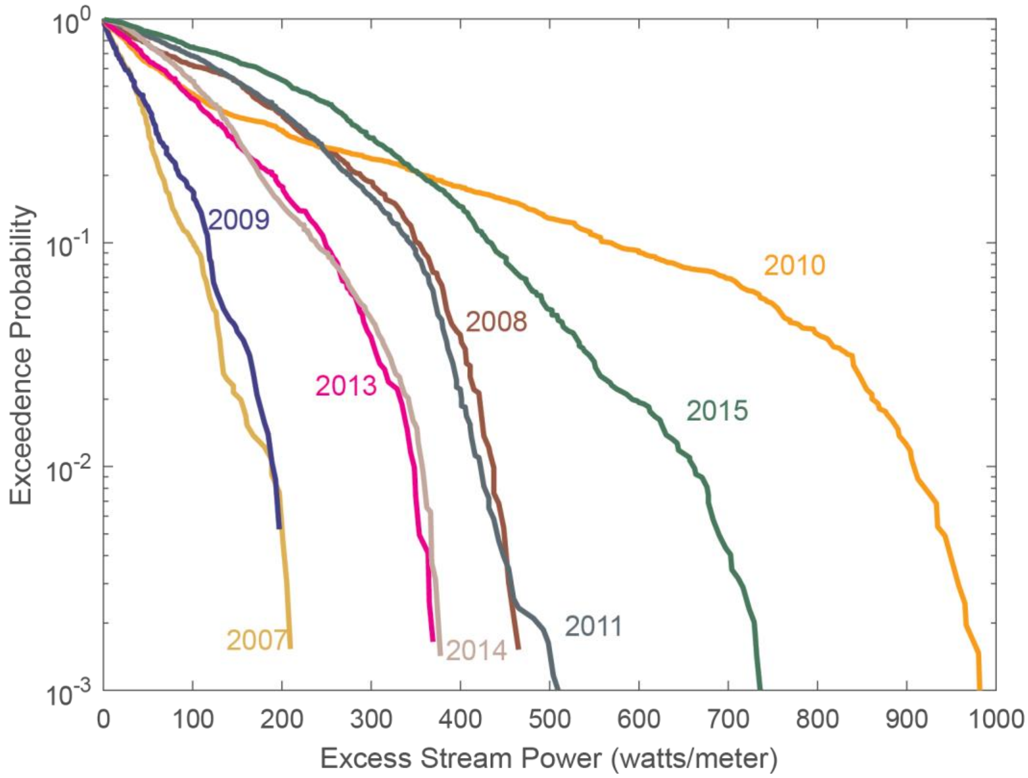

Figure 14. Exceedance probability plots of excess stream power provide a way to gauge the transport potential of annual runoff hydrographs that takes into account both flood intensity and duration. 2012 is not plotted because the flow never exceeded the transport threshold.

Tracer Displacement

To calculate the streamwise dispersion of the tracer cloud, the Cartesian tracer positions were converted to a streamwise and stream-normal coordinate system using the method described by *Legleiter and Kyriakidis* [2006]. The streamwise tracer displacement was calculated over all pairs of years between May 2007 and the end of the 2015 flood.

Equation 8

$$\langle \Delta s_{ij} \rangle = \frac{1}{N_k} \sum_{1}^{N_k} \Delta s_{k,ij}$$

Where where $\Delta s_{k,ij}$ is the streamwise displacement of the k^{th} tracer from year i to year j andN_k is the total number of tracers recovered in both years.

Sediment Flux Averaging

To compare tracer transport to the model sediment flux, I needed some representation of sediment flux over the whole model, such as the average. But is that a reasonable approach, given that the model does not perfectly conserve sediment mass? A sediment flux of 10^{-6} m^3/s corresponds approximately to a 1 cm^3 particle in motion, so in a system such as Halfmoon Creek where sand is mostly absent from the surface layer (see Figure 3), fluxes less than about 10^{-7} m^3/s can be ignored, especially since I am concerned only with the sediment in the tracer grain size class, 45-64 mm. Figure 15 shows the cumulative distribution of sediment fluxes in this grain size class across the model inlet, outlet, and all monitoring lines for a low flow year, 2009, and the highest flow year, 2010. The black line in Figure 15 is the CDF is the average of all the sediment flux time series. Fluxes over the entire model run greater than about 10^{-7} m^3/s range over less than 1 order of magnitude and a distributed approximately symmetrically around the average flux. This suggests that the average of all monitoring line sediment fluxes for a simulated flood is a reasonable representation of the "actual" model flux if mass were conserved and the flux varied smoothly with discharge. The average sediment flux for a flood was computed by averaging all the monitoring line flux timeseries to a single average flux timeseries and then taking the average of that for single average value, $\overline{Q_s}$ [m^3/s]. A second annual average flux, $\overline{Q_{stot}}$ [m^3/yr] was computed from the N monitoring line sediment totals (Equation 5), $\overline{Q_{stot}} = (\frac{1}{N}) \sum_{k=0}^{N} V_{s_k}$.

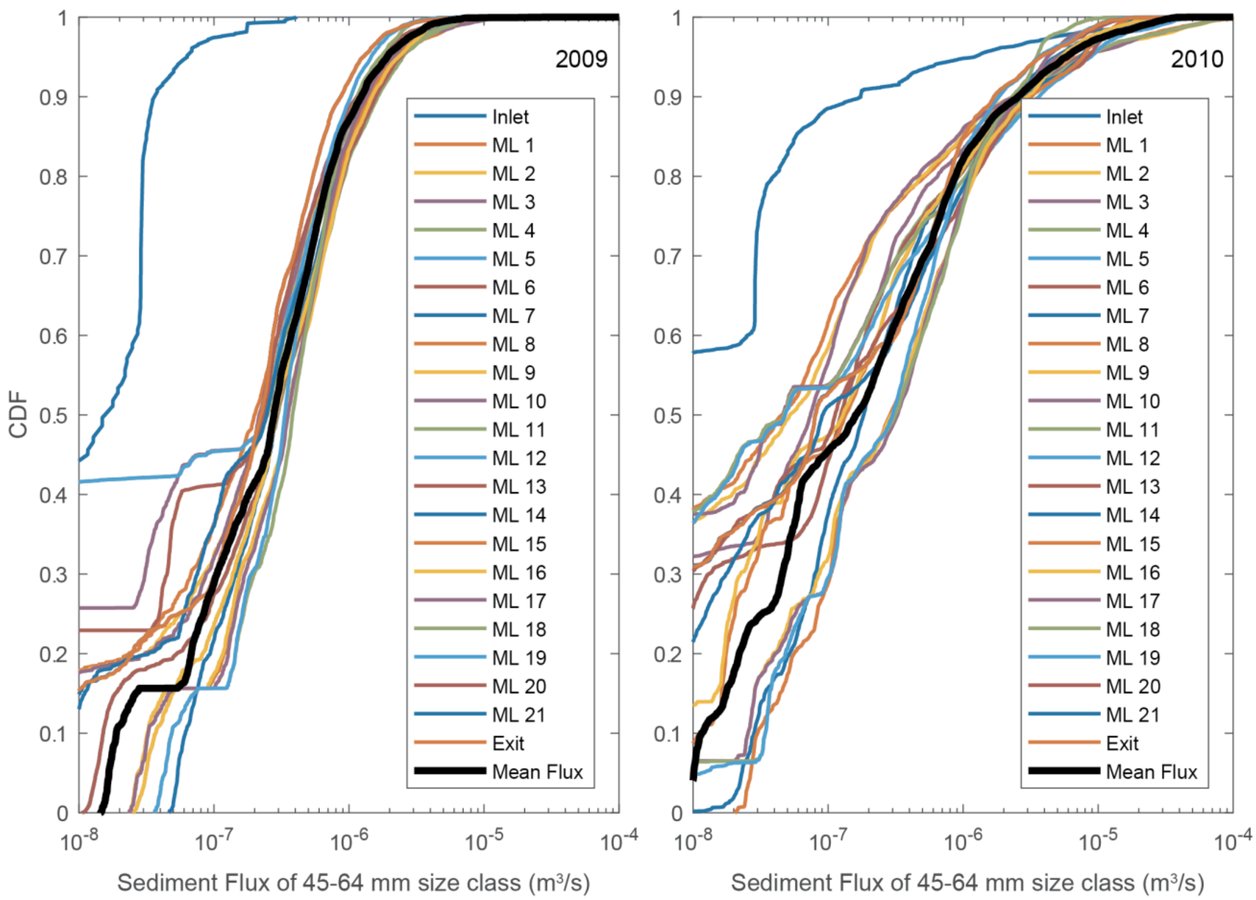

Figure 15. The cumulative distribution of sediment fluxes for a low flow year, 2009, and the highest flow year, 2010. Fluxes greater than about 10^{-7} m^3/s range are well represented by the average flux, shown as a solid black line in both plots.

Sediment flux predicted by tracer travel distance

One of the main reasons to study the movement of individual particles in streams is to estimate the bedload transport. While the motion of individual particles is highly stochastic, the transport rate can be estimated from the average motion of the tracer population. The lengths of individual particle displacements provide a link between the Lagrangian and Eulerian frameworks (Einstein 1937; Crickmore & Lean 1962; Hubbell & Sayre 1964).

Wong et al. (2007; see also Crickmore et al. 1990) detailed three methods for calculating sediment transport using tracer data. The one I will use relates the volumetric sediment transport rate to the product of the volume of sediment entrained per unit time per unit area, $\dot{e}$, and the mean particle step length, L_s

Equation 9

$$q_s = \dot{e} L_s$$

Phillips et al. [2013] found a linear relationship between time-integrated excess shear velocity and mean tracer transport. Shear velocity is similar to stream power in that it is a representation of the hydraulic forcing that drives sediment transport, so I expected to find a linear relationship between mean tracer displacement L_s and cumulative excess energy of the form

Equation 10

$$L_s = aE_t + b$$

where E_t is given by Equation 6, and a and b are the slope and intercept of the linear relationship. Substituting Equation 10 for L_s in Equation 9 yields a prediction of the average model sediment flux as the product of erosion rate and the tracer transport distance in response to forcing E_t.

Equation 11

$$\widehat{q_s} = \dot{e}(aE_t + b)$$

The erosion rate $\dot{e}$ I used is the average value of the time series of spatially averaged erosion rates that SRH-2D writes to the *_ERO.dat file.

To test Equation 11, it is necessary to convert the total average model flux for each year, $\overline{Q_s}$, to unit fluxes by dividing by the average channel width w. To compute a time series of average channel width, I computed the wetted area in the model at each time step, A_w, and divided it by the streamwise length DS of the model river $w = A_w/DS$ to yield a time series of average width. The average unit sediment flux is $\overline{q_s} = \overline{Q_s}/w$.

Patterns of Erosion and Deposition

I compared patterns of tracer concentration change to the patterns of bed elevation change (erosion and deposition) predicted by the model. The tracer concentration C is defined as the number of tracers N in a given area A

Equation 12

$$\boldsymbol{C_i = N_i/A_i}$$

where the indexing subscript refers to i^{th} polygon, which could be as small as a model mesh cell. However, using model mesh cells makes meaningful comparison difficult because mesh cells are much smaller than the geomorphic features in the stream. Larger polygons average tracer concentration and erosion (or deposition) over a larger area, making comparison more meaningful. To construct these polygons, I created a new mesh with approximately half the number of channel elements so that each polygon is a roughly twice the area of a model mesh element.

The tracer concentration change over the course of a flood in year j is simply the difference from the previous year.

Equation 13

$$dC_{i,j} = C_{i,j} - C_{i,j-1}$$

The modeled bed elevation change for the i^{th} polygon is $dz_i = -e_i$ where $-e_i$ is the erosion depth reported by SRH-2D for all model mesh cells that fall within the polygon.

To compare the similarity of the spatial patterns of tracer concentration change and bed elevation change, I classified tracer concentration change and bed elevation as depositional, no change, or erosional, indicated by 1, 0, and -1 respectively. The similarity of the type of bed elevation change and tracer concentration change (denoted as η) is indicated by the similarity index κ

Equation 14

$$\kappa_i = \eta_{dC,i} - \eta_{dz,i}$$

The value of κ ranges between -2 and 2. The meaning of each value is shown Table 3. Using the similarity index, I also calculated the fraction of area within each numbered polygon in Figure 13 that has a matching category, e.g. $\kappa = 0$.

Table 3. The meaning of possible values of the similarity index *S*.

		Bed Elevation		
		Deposition (1)	No Change (0)	Erosion (-1)
Tracer	Deposition (1)	0	1	2
	No Change (0)	-1	0	1
	Erosion (-1)	-2	-1	0

Results and Discussion

Conservation of Model Sediment Mass

As configured for the model runs described above, SRH-2D does not conserve sediment mass. Much of the effort in this research project went into confirming this and trying to understand the causes. I am confident that my results are accurate, but I do not have any great insight as to the cause.

Figure 16 shows the imbalance between sediment in transport or leaving the model and the sediment supply. The left hand side of Equation 3 (sediment in plus sediment eroded from the bed) is plotted in blue and the right hand side (sediment out plus sediment in transport) is plotted in red. The blue and red plus signs are the inlet and outlet sediment flux as reported by SRH-2D in the *_OUT.dat file and serve as a verification that the technique for integrating the monitoring line sediment flux is correct.

It is clear from Figure 16 that there is significantly more sediment (up to about three times more) leaving the model than is supplied by the inlet boundary condition and erosion of the stream bed. Somehow, the model is “creating” sediment. It is possible that the sudden spikes in sediment flux shown in Figure 11 are the origin of this excess mass. This possibility could be investigated further by integrating under the spikes in Figure 11 and comparing this mass to the overall model mass imbalance.

The sum of the sediment sources (the left hand side of Equation 3, plotted in blue) is fairly systematic with the size of the flood. The floods of 2007 and 2009 were small and very similar, and the amount of sediment entering the model and eroded from the bed is about the same in both model years. The floods of 2010 and 2015 were the two largest and resulted in the largest sum of inlet boundary and eroded sediment.

The amount of sediment represented in the right hand side of Equation 3 does not vary as systematically with flood size as the left hand side. The amount of extra mass is greater in high flow years (2008, 2010, 2011, and 2015) than in low flow years (2007, 2009, 2012, 2013, and 2014), but the pattern of mass imbalance is complex. For example, 2010 was the largest flood during the study (see Figure 14), but the floods in 2011 and 2015 “created” more sediment. The larger floods of 2008 and 2011 were nearly identical in terms of the amount of excess stream power, but the sediment imbalance is greater in 2011. Similarly, the floods of 2013 and 2014 were nearly identical, yet the 2014 model run “created” approximately four to five times as much sediment as the 2013 model run.

To further investigate origin of the anomalous mass, I examined mass conservation at the spatial resolution of the monitoring lines and polygons shown in Figure 13 using the divergence of flux formulation given by Equation 5. Figure 17 and Figure 18 show the mass balance for two low flow years (2007 and 2009) and two high flow years (2010 and 2015 The left hand side of Equation 5, the divergence of flux across two successive monitoring lines, is plotted in red. The right hand side of Equation 5, the sum of bed erosion and sediment in the water column in the polygon, is plotted in blue.

The pattern of mass imbalance in the two low flow years (Figure 17) is consistent. Mass is created (the left hand side of Equation 5 is greater than the right hand side) in polygons 1, 4, 7, 11, and 17. Small amounts of mass are lost in polygons 2, 5 and 16.

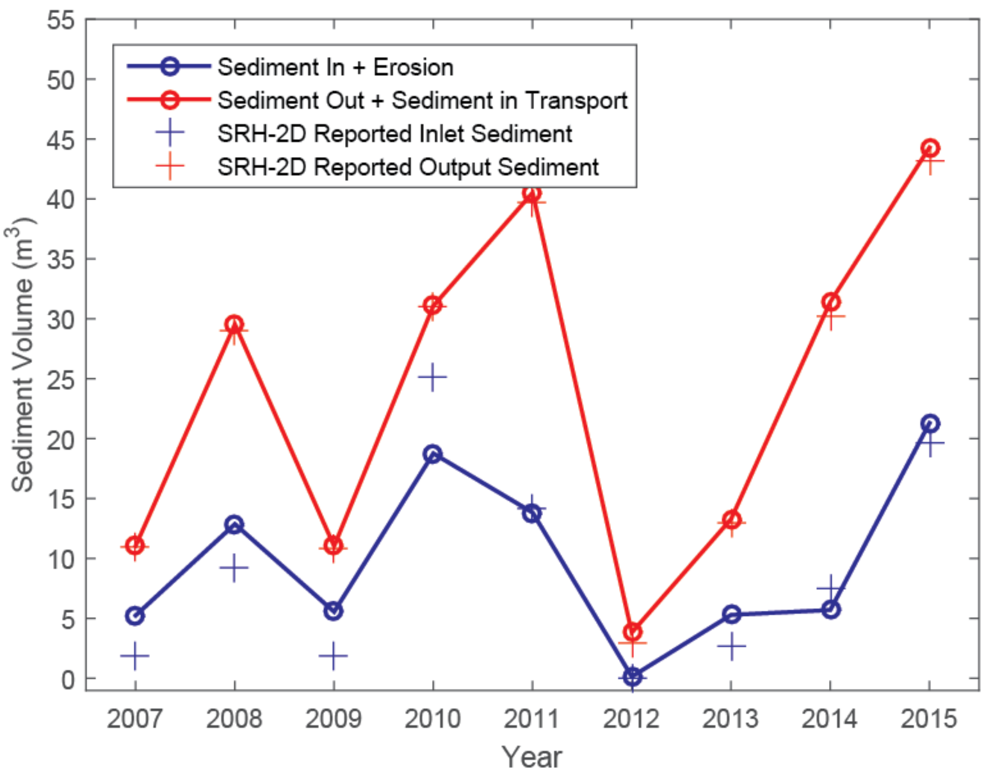

Figure 16. The sediment imbalance for each year. The red line is the sum of sediment crossing the model outlet and sediment in transport. The blue line is the sediment flowing into the model plus sediment eroded from the bed. If mass were conserved (Equation 3), the two curves would be identical. The difference between the red circles and the red plus signs is some combination of the amount of sediment in transport and rounding when writing the output text file.

The mass imbalance for the two high flow years (Figure 18) is mostly consistent, differing only in two polygons towards the downstream end of the model. A small amount of mass was lost from polygon 17 in 2010 and created there in 2015. Polygon 21 was more or less in balance in 2010, but in 2015, approximately 10 m^3 of sediment were “created” there. However, in both years, the majority of the extra sediment is “created” in polygons 11 and 12. This raised the question of whether mass was flowing across the neck of the meander from polygons 5 and 6, which lost mass, into polygons 11 and 12. To investigate this possibility, I created a north-south oriented monitoring line running parallel to the stream along the neck of the meander. In 2010, a total of 1 m^3 crossed the monitoring line. In 2015, about 0.6 m^3 crossed the monitoring line. The total amount of excess sediment appearing in polygons 11 and 12 is about 25 m^3 in both years, far greater than the amount flowing across the meander neck.

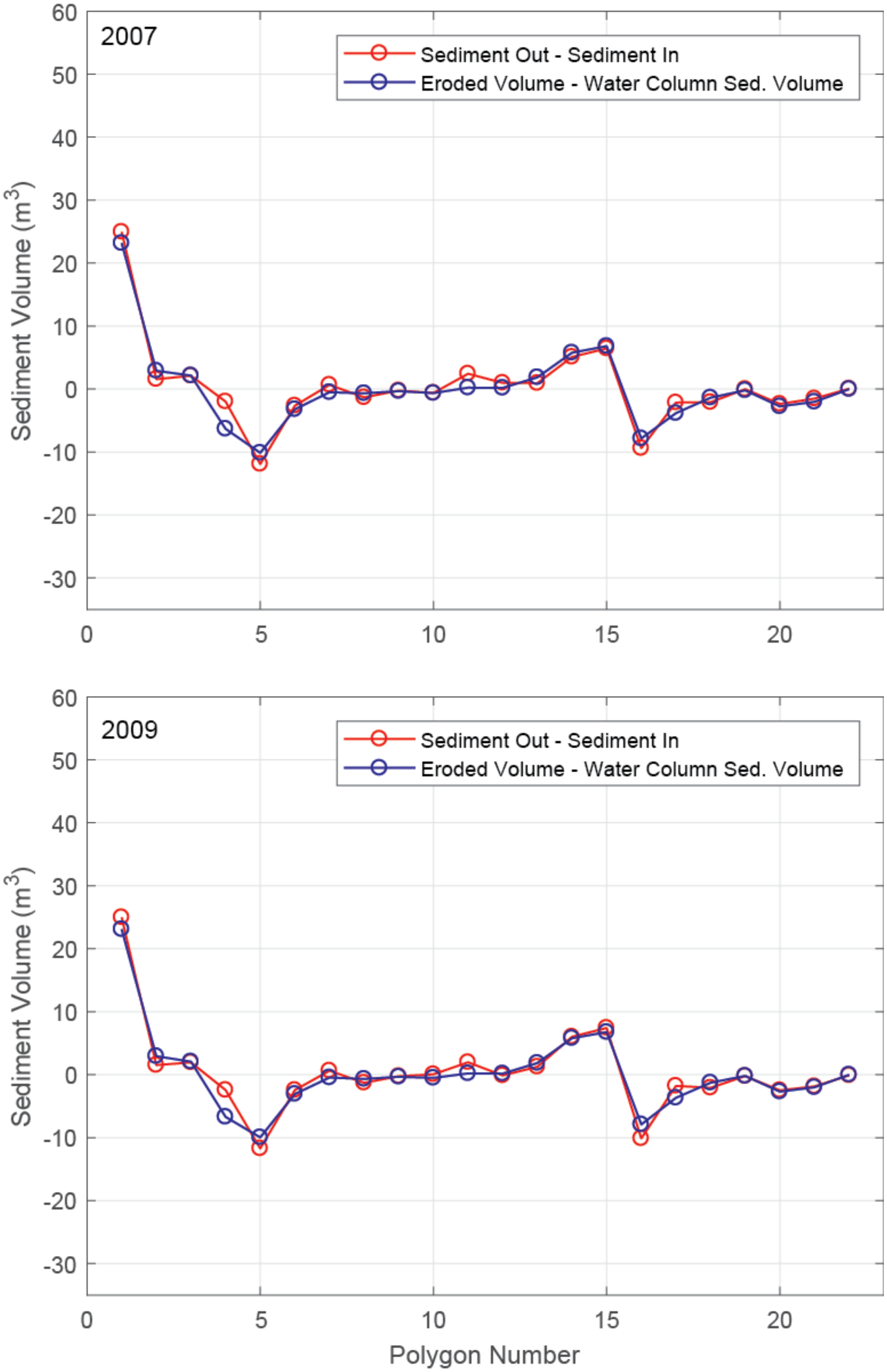

Figure 17. The change in sediment flux between successive monitoring lines compared to the amount of sediment eroded between them for two low flow years, 2007 and 2009.

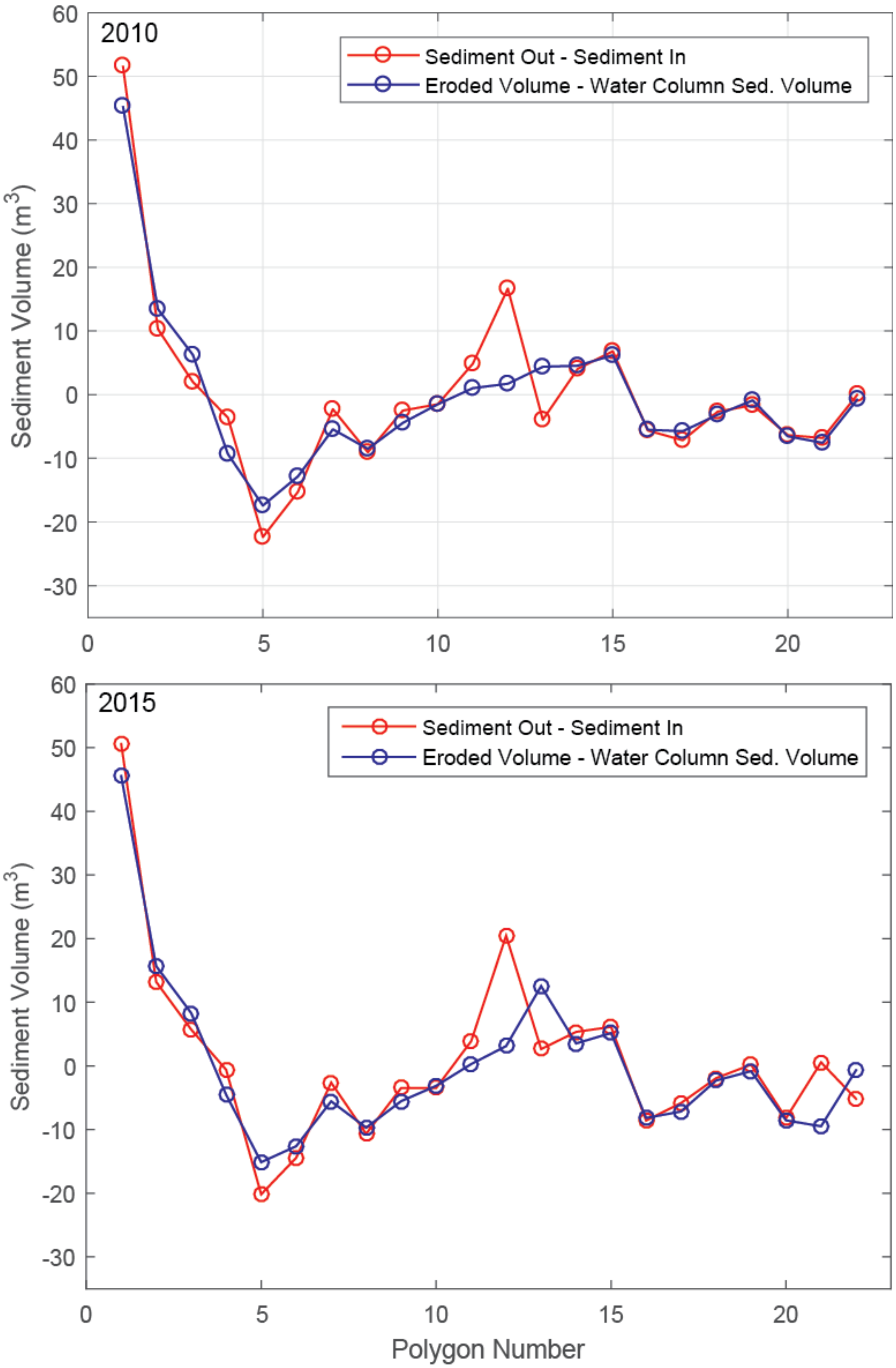

Figure 18. The change in sediment flux between successive monitoring lines compared to the amount of sediment eroded between them for two high flow years, 2010 and 2015.

Figure 19 shows the two sides of Equation 5 plotted for two moderately sized floods, 2013 and 2014. The patterns of mass gain and loss are similar, but the amount of excess mass in polygons 11 and 12 is greater in 2014. Polygon 13 lost a small amount of mass in 2013 but gained a more than 10 m^3 in 2014. One consistency in all of the years is that the amount of excess mass peaks in or around polygons 11 and 12 and mass is lost from polygon 5 in all years. This is a hint that the mass conservation problem may be related to particulars of the model mesh or the stream geometry and should be investigated further. The problem does not appear to be a numerical instability that can be eliminated by reducing the timestep size. Figure 20 shows Equation 5 plotted for 2 simulations of the 2015 flood. Reduction of the timestep from 5 seconds to 1 second yielded only marginal improvement.

Can SRH-2D replicate observed patterns of bedload tracer dispersion?

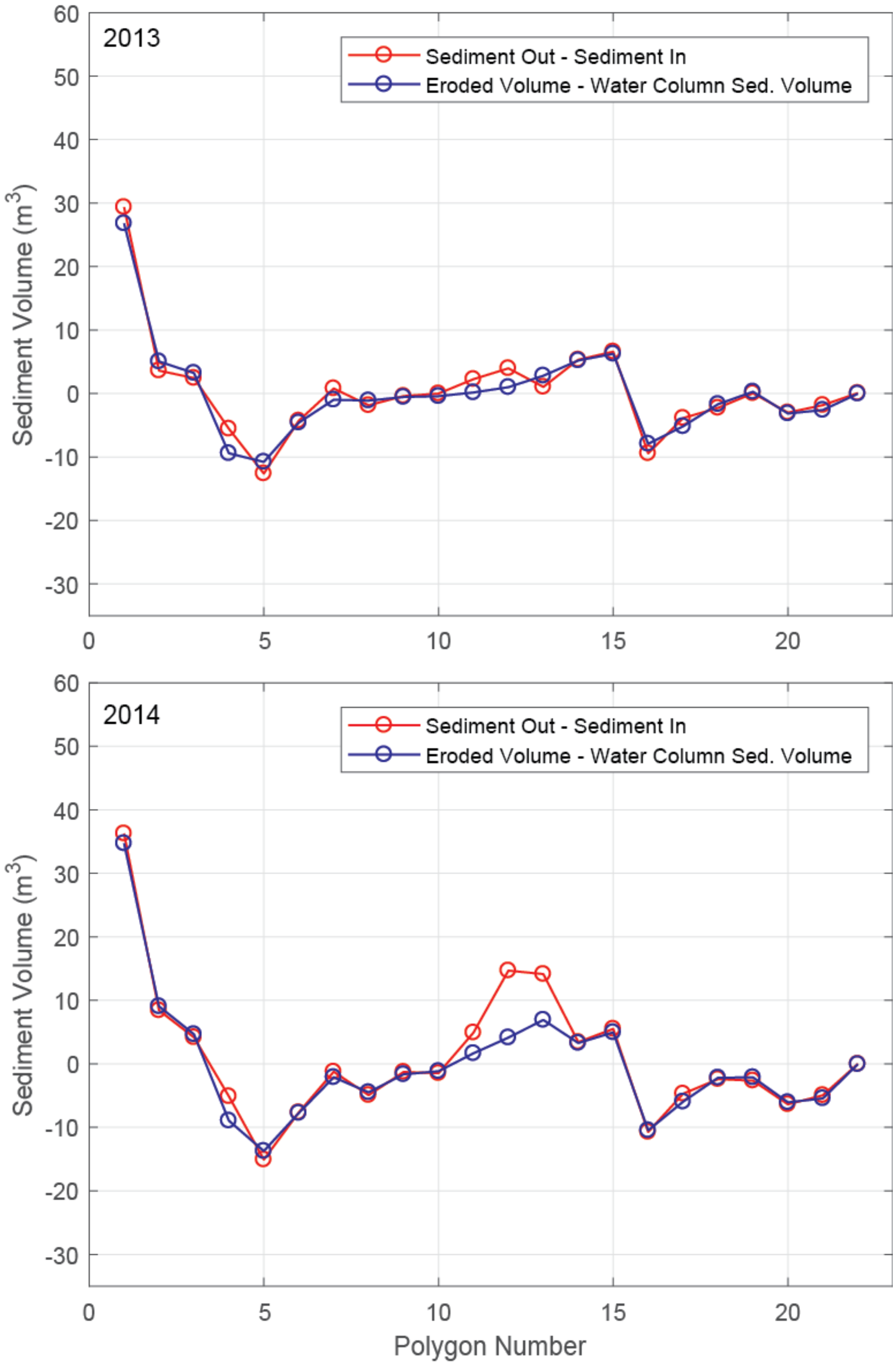

Figure 19. 2013 and 2014 were very similar floods (see

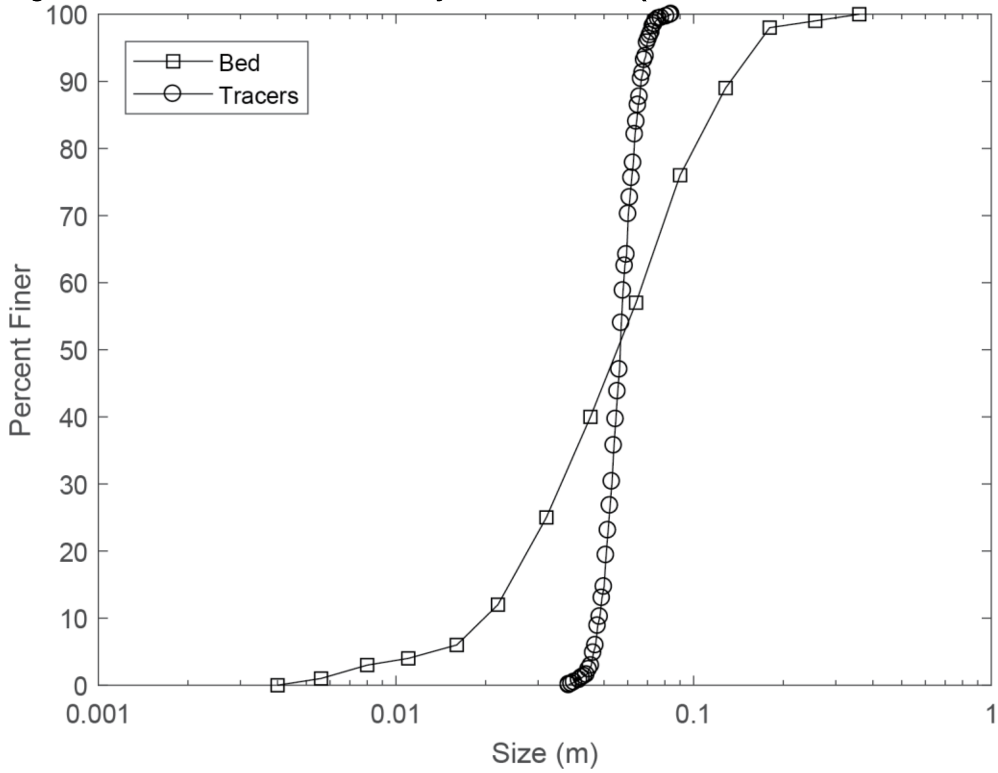

Figure 2 and Figure 14), but the scale of the violation of sediment mass conservation is greater in 2014.

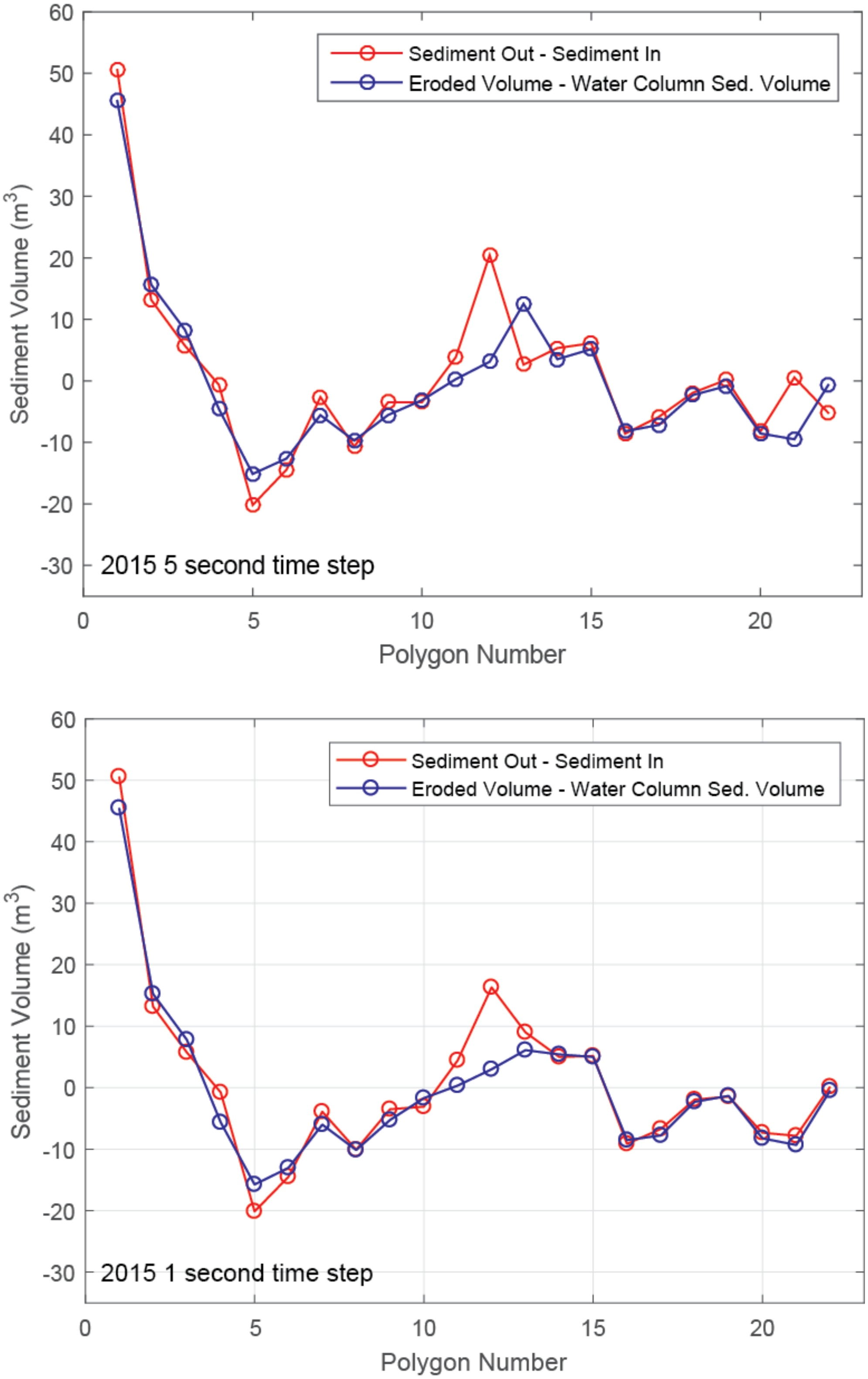

Figure 20. Reduction of the time step size from 5 seconds (top) to 1 second (bottom) does not improve the discrepancy in sediment mass conservation.

Comparing Model Sediment Flux to Tracer Travel Distance

Figure 21 shows the average annual modelled sediment flux in the tracer size class (45 – 64 mm) and average tracer displacement length plotted for each year. Mean tracer displacement ranges from about 10 m to almost 200 m. Mean annual sediment flux $\overline{Q_s}$, calculated as described in the methods section, ranges from about 1 m^3/year to about 10 m^3/year. The correspondence between the observed tracer transport and the averaged model sediment flux is remarkable, considering that the model does not perfectly preserve mass and that the flux is averaged over the inlet, the exit, and 21 monitoring lines. This is particularly true from 2007 to 2012. For the final three years of the study, the tracer transport distances are lower than would be expected from the first part of the study. For example, the 2013 and 2014 floods were larger than the 2007 and 2009 floods, yet the tracer transport was similar to those years. The 2015 flood was the second largest of the study, yet mean displacement was similar to the smaller flood of 2008. I attribute the tracer slowdown to burial in the stream bed and stranding high on bars during the high transport years of 2010 [e.g. *Ferguson et al.*, 2002; *Judith K. Haschenburger*, 2011a].

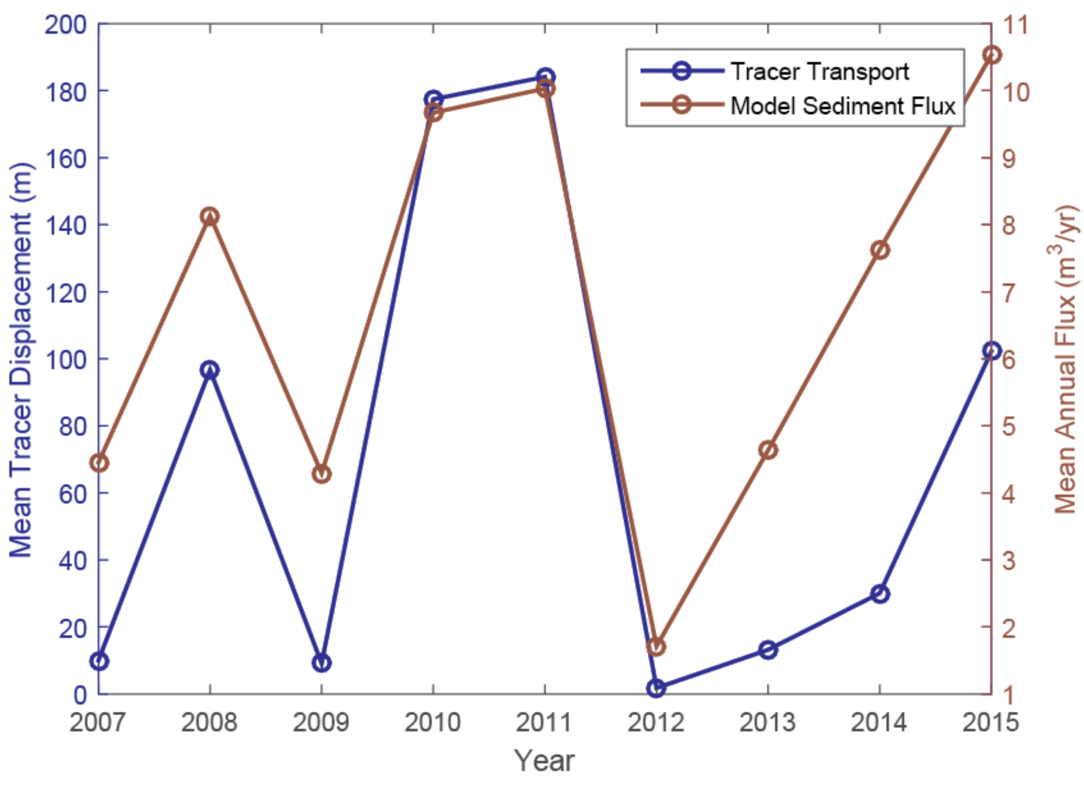

Figure 21. Mean annual tracer displacement compared to the model mean annual sediment flux. The model fluxes closely mimic the trends in tracer transport.

Linking Model Sediment Flux to Tracer Travel Distance

The similarity in the patterns of mean tracer displacement and mean annual model sediment flux is interesting, but these two transport metrics are not directly comparable because sediment flux and tracer travel distance have different units and because they represent the Eulerian and Lagrangian frameworks, respectively. Equation 9 provides a linkage between the two frameworks.

Phillips et al. [2013] showed that mean tracer displacement scaled linearly with cumulative dimensionless excess impulse, which they defined as time integrated excess shear velocity. I used a similar measure of hydraulic forcing, cumulative excess energy (E_t, Equation 6). Figure 22 shows that mean tracer displacement scales linearly with E_t

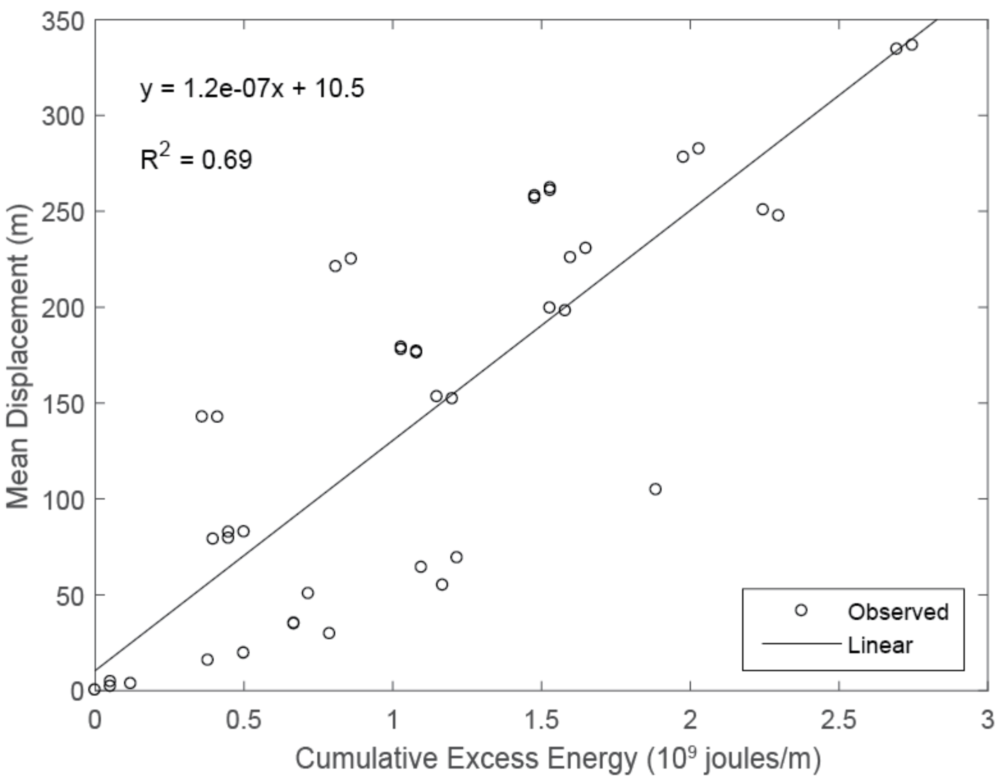

Figure 22. The mean tracer transport distance scales linearly with cumulative excess energy.

The slope and intercept of the linear regression in Figure 22 (a and b in Equation 11) provide the linkage between the tracer displacement as a function of excess energy and the model sediment flux. Figure 23 shows that the modeled average unit sediment flux $\overline{q_s}$ plotted as open circles, also scales linearly with excess energy. The predicted model sediment flux $\widehat{q_s}$ (Equation 11) is plotted as plus signs. The error in the predicted value, expressed as a percentage

$(\widehat{q_s} - \overline{q_s})/\ \overline{q_s}$ (the predicted value minus the model value divided by the model value), is shown in Figure 24. For all years, the predicted flux is within a factor of 2 of the modeled flux. Given the close correspondence between sediment flux and tracer transport distance shown in Figure 21, it is not surprising that there is a linear relationship between observed flux and excess energy. It is surprising that the magnitude of the flux $\widehat{q_s}$ predicted by Equation 11 is so similar to the average model flux, $\overline{q_s}$. Sediment transport is a highly non-linear process and sediment transport models often differ from observed fluxes by orders of magnitude [e.g. *Wilcock and Crowe*, 2003], so this result should be viewed with some skepticism. A test with a second tracer data set and transport model is warranted.

If the success of predicting model sediment flux from tracer travel distance is not a spurious correlation, coincidence, or fluke, it implies that erosion rates and fluxes from SRH-2D could be used to predict tracer transport distances, if the physical meaning and values of a and b in Equation 11 can be determined. The meaning of b is straightforward. It is the average displacement at zero excess energy, so it should generally be equal to 0 if all tracers start in the same position. It is non-zero in this case because the tracer population was initially spread out over about 28 m of stream, with an average initial position of about 14 m (which is not too different from the regressed intercept, 10.5 m). The meaning of a is less obvious. Dimensional consistency dictates that a has SI units of m^2/joule, which suggests that it is transport response to a joule of excess hydraulic forcing. As such, the value of a would be expected to be grain size and bed texture dependent. Further research to constrain this parameter could allow SRH-2D to be used to predict the transport distance of augmented gravel.

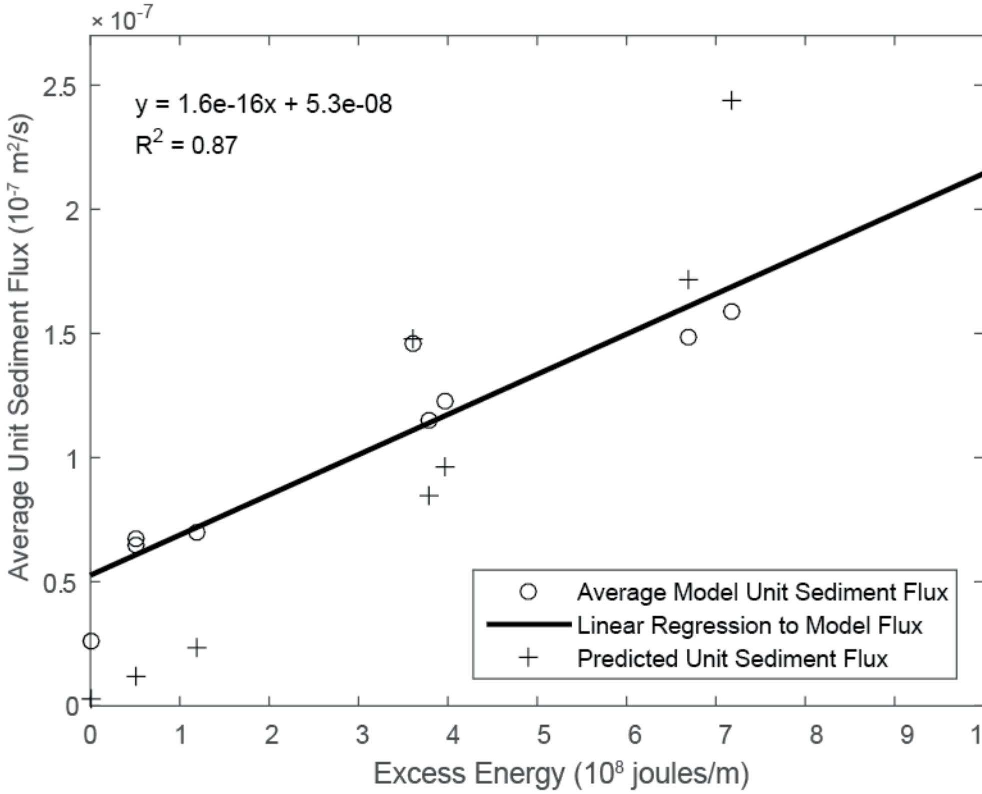

Figure 23. The average model unit sediment flux $\overline{q_s}$ (open circles) scales linearly with the excess energy in each flood. The plus signs are the flux $\widehat{q_s}$ predicted by Equation 11.

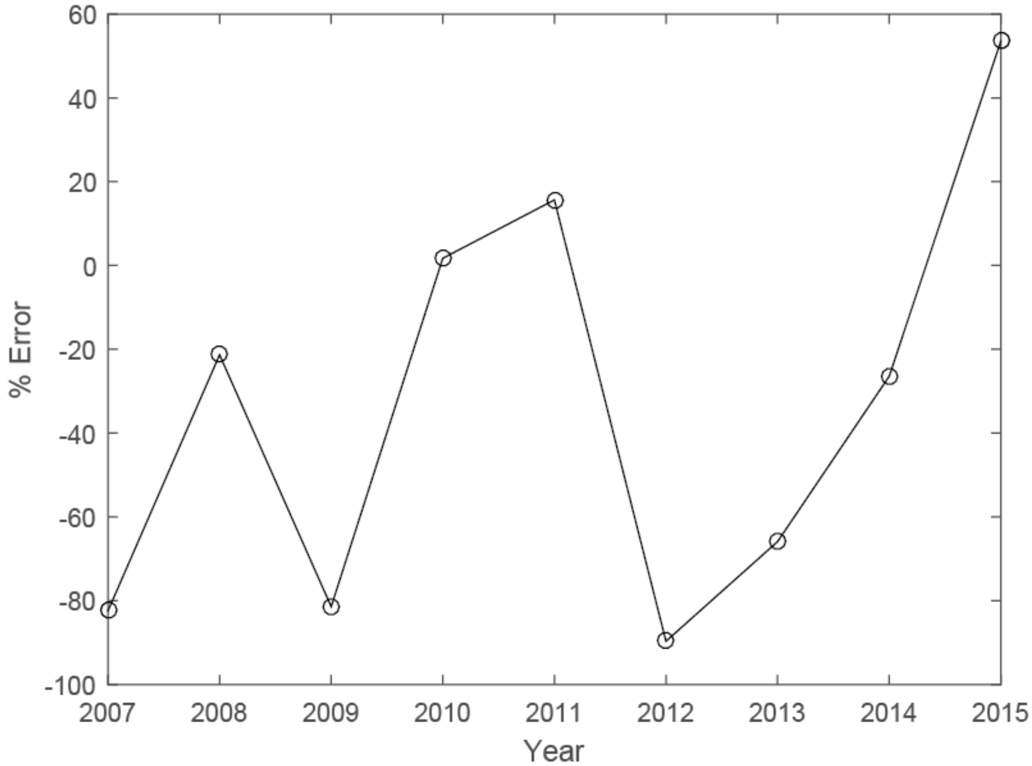

Figure 24. The percent error $(\widehat{q_s} - \overline{q_s})/\ \overline{q_s}$ in the model sediment flux $\widehat{q_s}$ predicted by Equation 11.

Patterns of Erosion and Deposition

In this section, I compare the model patterns of erosion and deposition to tracer concentration change. For each flood, I present a map of tracer concentration change side by side with a map of model topographic change as a qualitative comparison. I attempt to quantify the similarity of the two maps, which I refer to as erosion/deposition maps, with a similarity index defined by Equation 14.

Figure 26 through Figure 42 show the erosion/deposition maps and the similarity index maps for each flood year. Warm colors in the erosion/deposition maps indicate tracer or model deposition and cool colors indicate erosion. The similarity maps display each of the 5 possible values with a different color. Matching areas are shaded light green. Areas shaded dark gray are those where tracer concentration change is undefined because no tracer occupied the area at the end of the current flood and the previous flood. The similarity figures also include a plot of the fraction of the area in each of the polygons defined by the monitoring lines (Figure 13) where the tracer concentration change category matches the model topographic change category.

Generally speaking, the spatial patterns of SRH-2D model topographic change are consistent from year to year and the scale of the change (both the amount of elevation change and the amount of area affected) increases with the size of the flood. The amount of erosion or deposition is generally less than about 20 cm, which was one of the goals of the inlet sediment flux boundary condition. The model predicts that much of the study area is depositional, with areas of erosion between the gravel bars. This is not an unreasonable result, but the amount of deposition is more than actually occurs in the river. The model results could probably be improved by modeling the entire flood sequence as one model run or by using the topography at the end of one flood as the starting conditions for the next flood. This might allow the model to reach the topographic quasi-equilibrium observed in the field.

The patterns of tracer concentration change are more complex than the model topographic change. The flood sequencing plays a role in tracer mobility (as tracers get more deeply mixed into the bed) and the interpretation of erosion and deposition patterns is complicated by the fact that the upstream supply of tracers changes throughout the study as tracers are distributed throughout the study reach.

The simplest example of this effect is shown in Figure 27. The 2008 flood deposited tracers all along the area upstream of the first meander bend, resulting in a broad area of agreement with the model, as shown in Figure 28. However, the tracer concentration change pattern could only have been depositional because no tracers occupied this area before the 2008 flood.

A more difficult case to interpret in light of the finite upstream tracer supply is the pattern of deposition around the first meander. The floods of 2008 (Figure 27) and 2010 (Figure 31) deposited tracers all around this bend. The 2011 flood was very similar to the 2008 flood (Figure 14), yet tracers were mostly eroded from this area (Figure 33). Clearly there were not enough tracers arriving from upstream to replace those that were eroded, many of which were deposited at the apex of the next bed (polygon 13). Why? There were more than 300 tracers (out of 893 total) upstream of the first meander bend at the beginning of the 2011 flood, as compared to 750 upstream of the meander bend at the beginning of the 2010 flood, so reduced availability of tracers could be the cause. However, the 2011 the mean tracer displacement was roughly 1/3 less than during the 2008 flood (Table 1.

Table 1), so perhaps tracers from upstream just didn't make it all the way to the bend. I favor the latter interpretation and I attribute the tracer slow down to tracer burial and stranding (on bars above the elevation of subsequent floods) by the large 2010 flood. This interpretation is supported by the increase in tracer concentration on the first meander during the 2015 flood, but tracer supply does play a role, because sediment transport is a stochastic process. Tracer entrainment, transport distance, and deposition are governed by probabilities and even if the probability distributions of each stage of tracer transport are the same for two floods, there will be less apparent transport if fewer tracers are available.

With that in mind, the similarity index plots show that the model topographic change matches the tracer concentration change best on the gravel bars (polygons 8 and 9, polygon 13, and polygon 17) and the correspondence is better during the higher flow years. Additional observations about the erosion/deposition maps and the similarity maps are included in the captions of Figure 26 through Figure 42.

One correspondence between the tracer concentration patterns and the model is not captured by the similarity index. The model predicts erosion in short sections between the depositional areas (e.g. Figure 33). In these areas, much of the tracer concentration change is undefined, because tracers move all the way through them during an episode of motion. This interpretation of the tracer behavior is consistent with the model prediction of an erosive area.

The erosion/deposition maps also do not reflect the maintenance of pools at the apexes of meander bends. For example, there are about four pools around the apex of the first meander (visible in Figure 5) that have persisted throughout the course of the study. The exact number, location, and depth varies from year to year Tracers are deposited in the pools and in the bed forms that separate the individual pools, but the pools existence is evidence that in general, they are not depositional. The model topographic change also does not reflect the maintenance of the pools. Instead, the model tends to fill pools. The mechanism(s) responsible for riffle pool maintenance is a long standing question in fluvial geomorphology [e.g. *Clifford*, 1993; *Milan et al.*, 2002] so it is not surprising that SRH-2D does not maintain pools. It is less clear how to interpret tracer deposition in pools.

The comparison of tracer concentration change and model topographic change is further limited by the fact that the model topographic change includes erosion or deposition of all grain sizes, whereas the tracer population is a narrow grain size distribution.

A final issue in comparing the tracer concentration change to the model topographic change is the choice of the spatial scale of comparison. I chose to use polygons derived from the model mesh that were approximately 4 m^2 in size. This size was chosen so that the morphologic features of the stream, such as a pool or the thalweg, would be resolved by at least one and likely more than one polygon. However, this choice introduces “noise” into the comparison if not all polygons representing a morphologic unit respond in the same way. On the other hand, polygons drawn much larger than the scale of the stream morphology might not reveal interesting small scale effects. A better approach might have been to draw custom polygons that represent each morphological feature of interest.

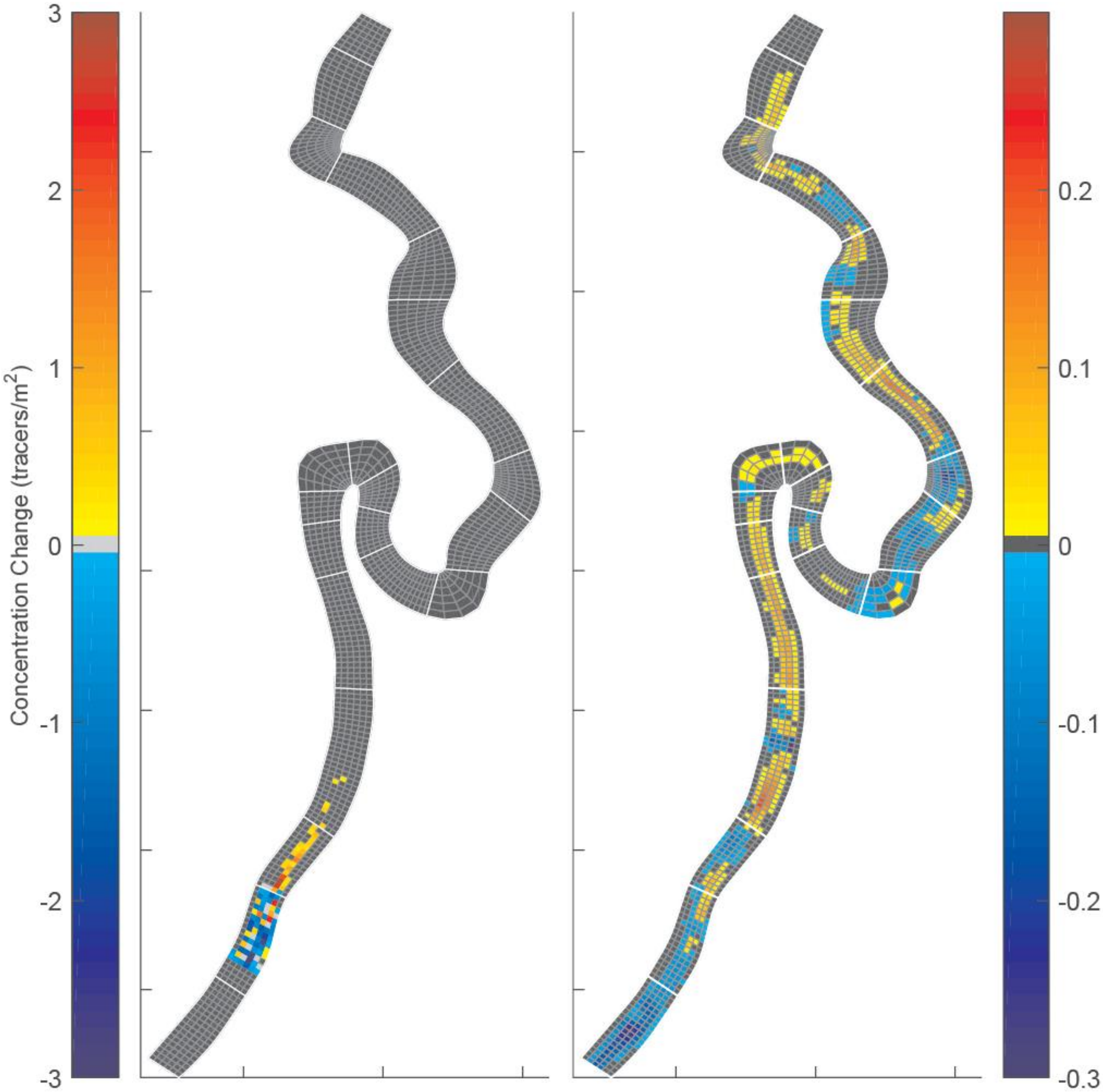

Figure 25. Maps of the 2007 tracer concentration change (left) and model bed elevation change (right).

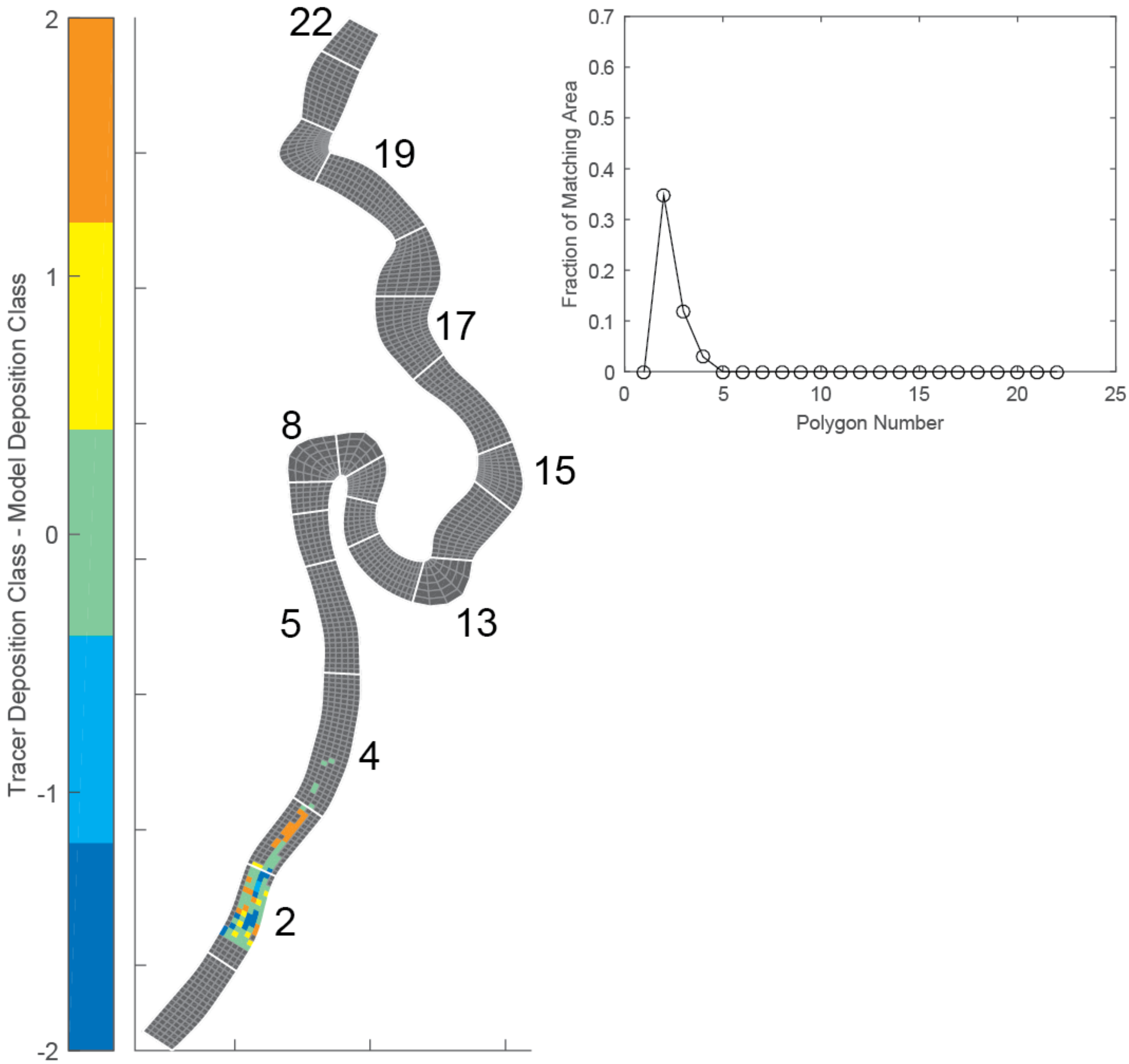

Figure 26. Map showing the 2007 erosion or deposition similarity index. The graph shows the fraction of matching area in each polygon.

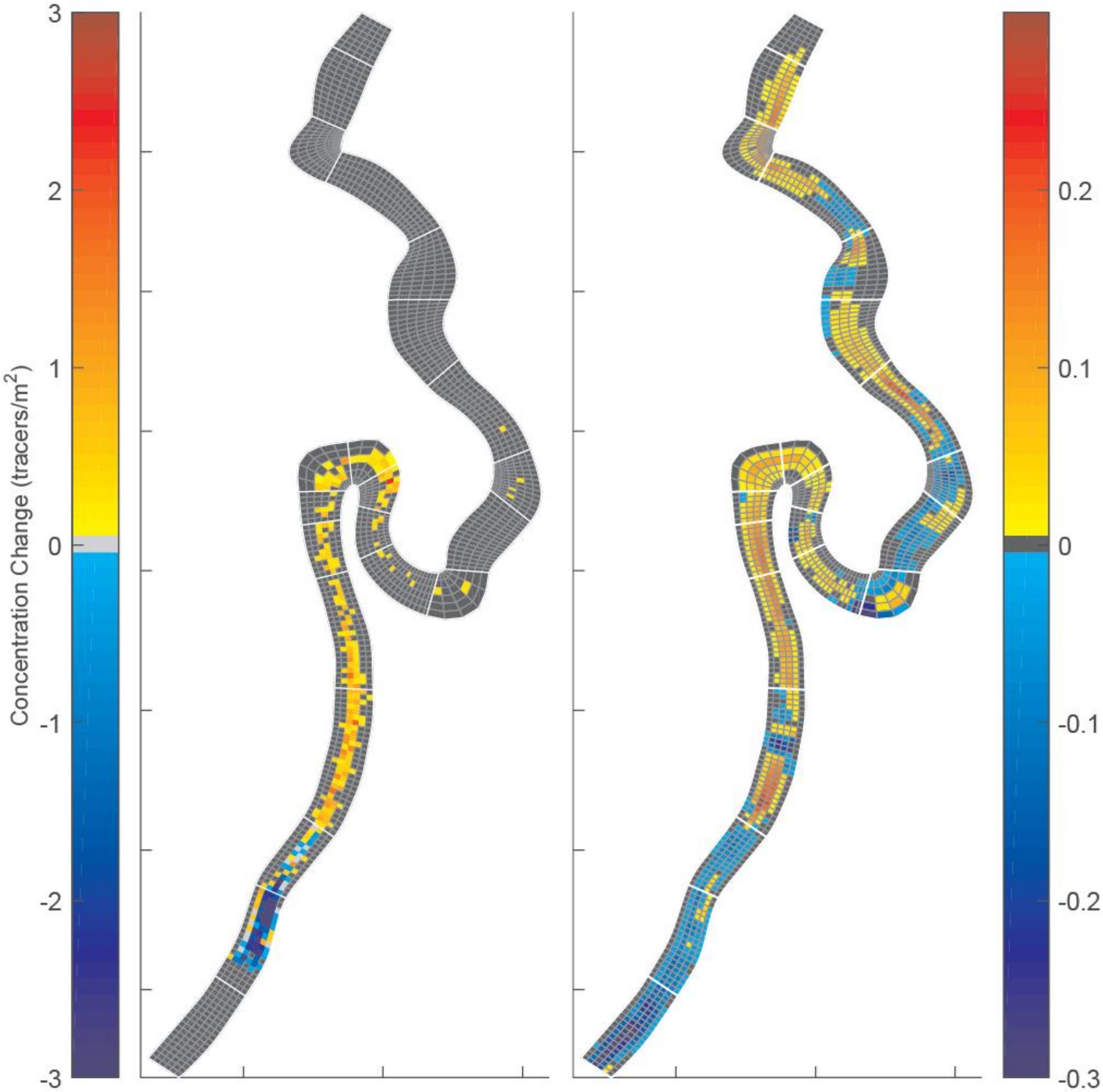

Figure 27. Maps of the 2008 tracer concentration change (left) and model bed elevation change (right) show broad areas of deposition. However, tracer deposition over most of the study area was the only possible outcome in this year.

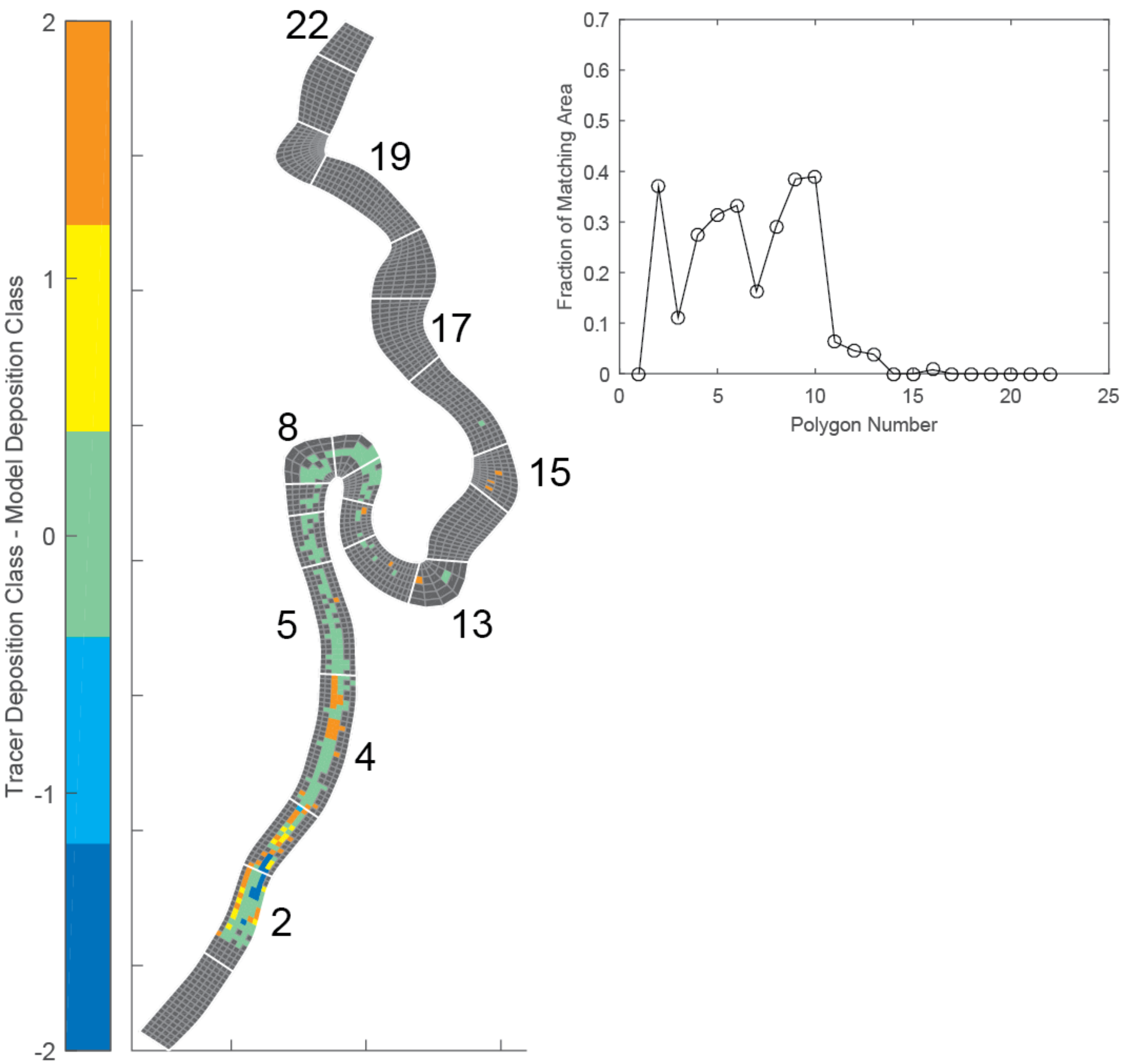

Figure 28. Map showing the 2008 erosion or deposition similarity index. The graph shows the fraction of matching area in each polygon. There is a substantial area of agreement in polygons 4 through 10, but this is due to the fact that tracer concentration change could only increase in an area where no tracers existed before.

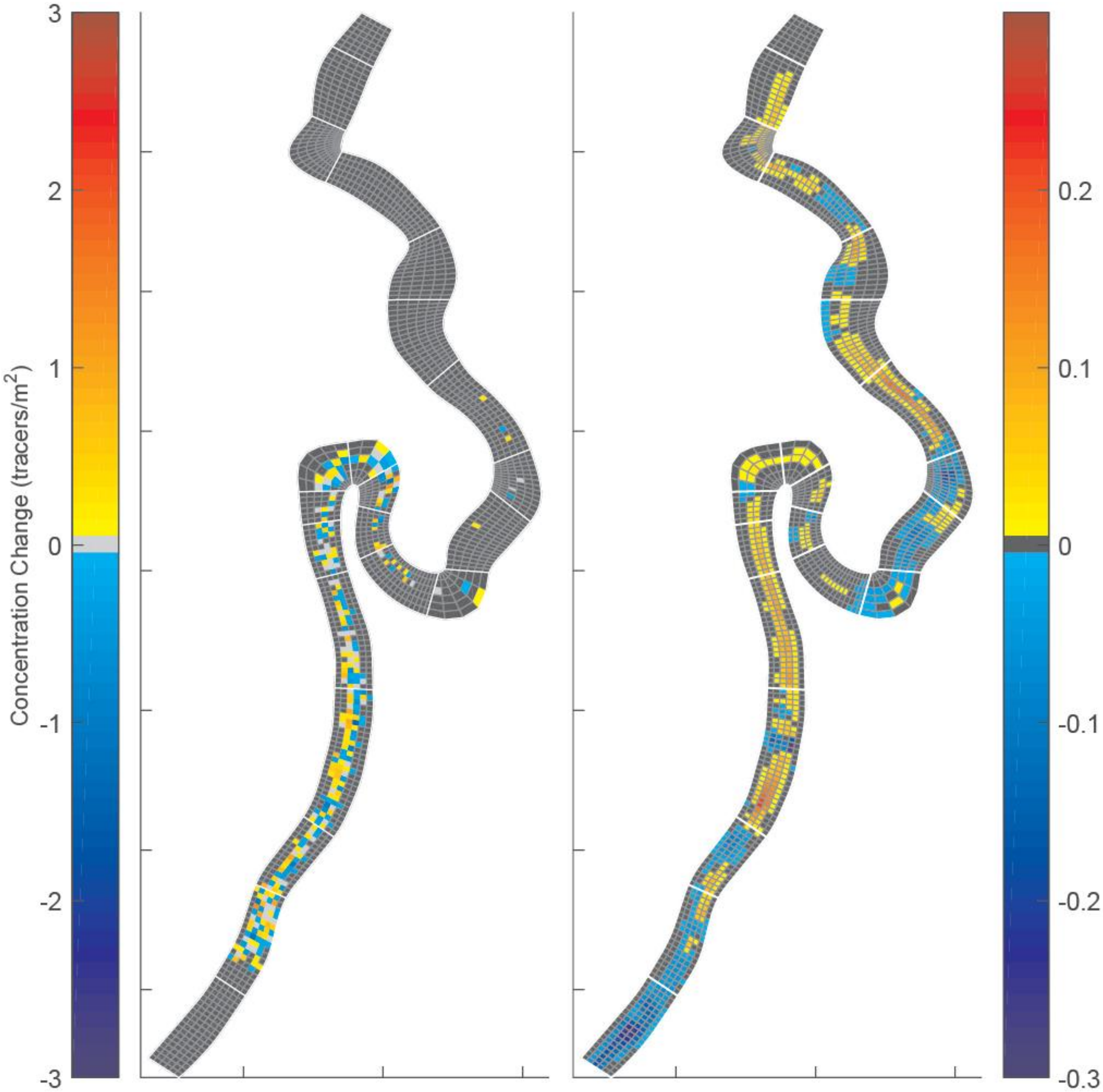

Figure 29. Maps of the 2009 tracer concentration change (left) and model bed elevation change (right). 2009 was a small flood that yielded no strong patterns of tracer concentration change.

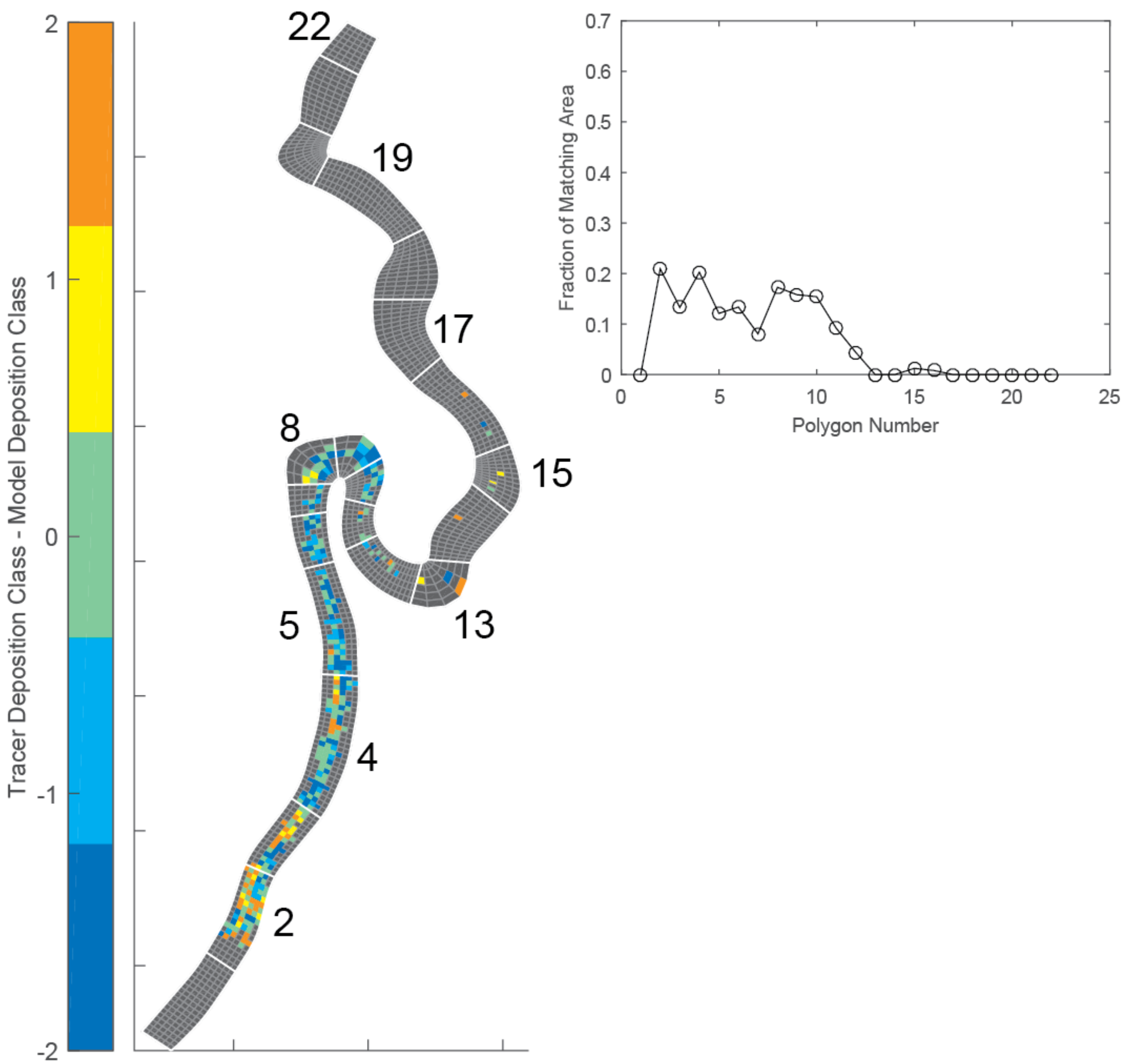

Figure 30. Map showing the 2009 erosion or deposition similarity index. The graph shows the fraction of matching area in each polygon. There is minimal agreement with no strong patterns.

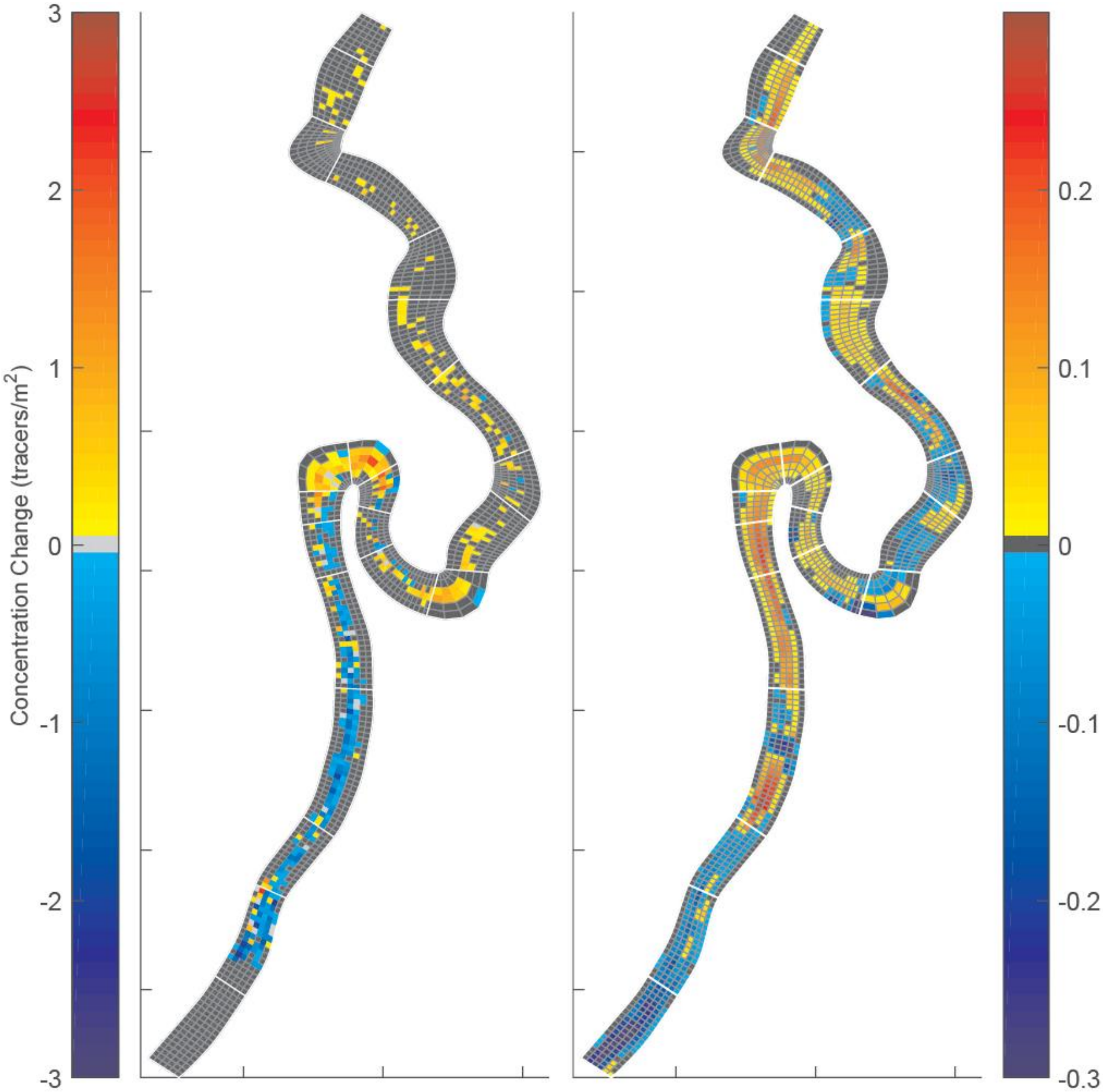

Figure 31. Maps of the 2010 tracer concentration change (left) and model bed elevation change (right). The 2010 flood deposited many tracers on the point bars of the first and second meanders. The model also indicated deposition in these areas. Upstream of the first meander, the model predicted deposition over a broad area where tracers were eroded. The model also predicted erosion on the upper part of the bar at second bend where tracers were deposited.

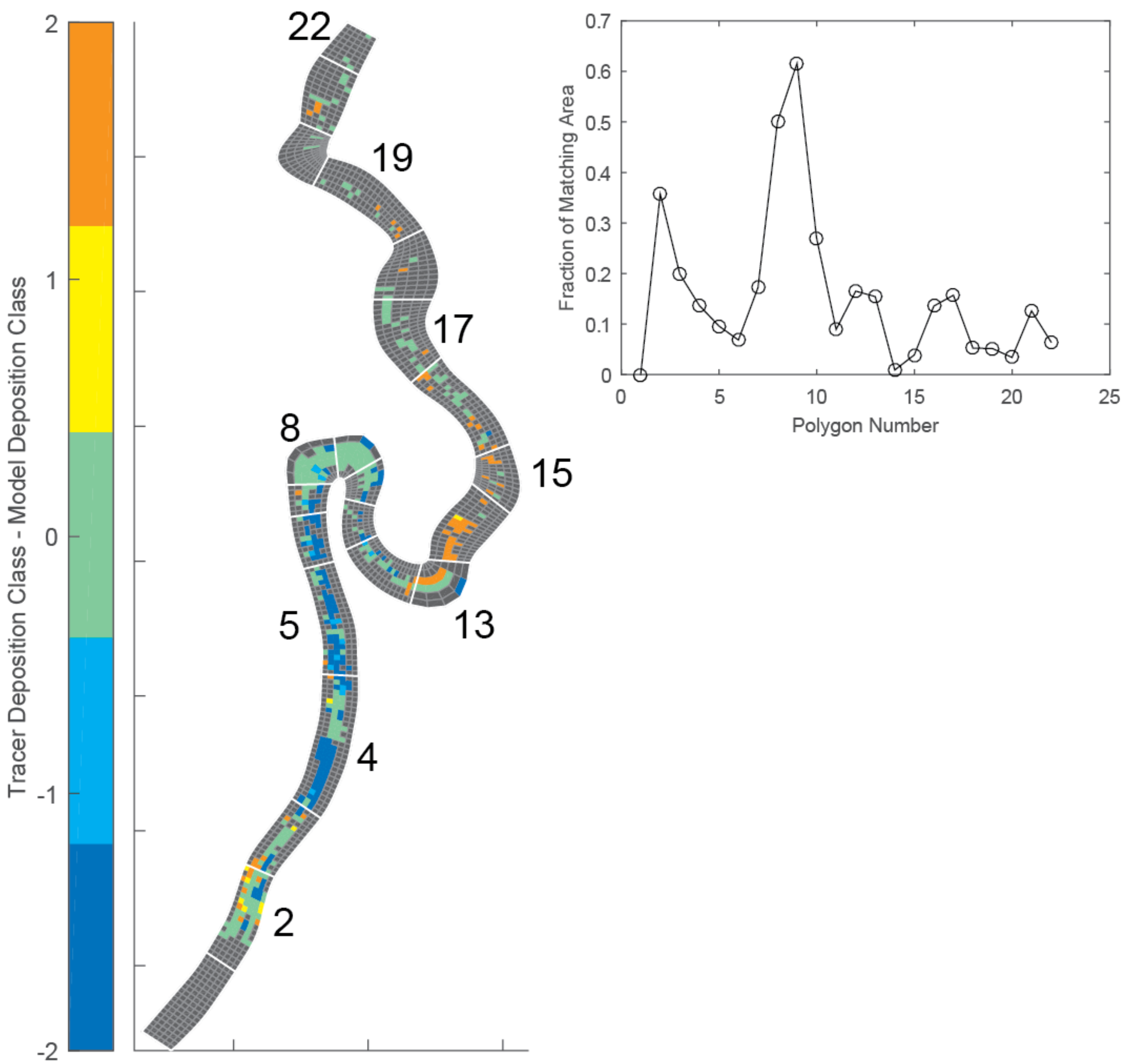

Figure 32. Map showing the 2010 erosion or deposition similarity index. The graph shows the fraction of matching area in each polygon. There is agreement in an area of erosion in polygon 2 and an area strong agreement in the depositional area around the first meander (polygons 8 and 9). Polygons 13 and 14 show strong disagreement (in orange) in an area where tracers were deposited but the model predicted erosion.

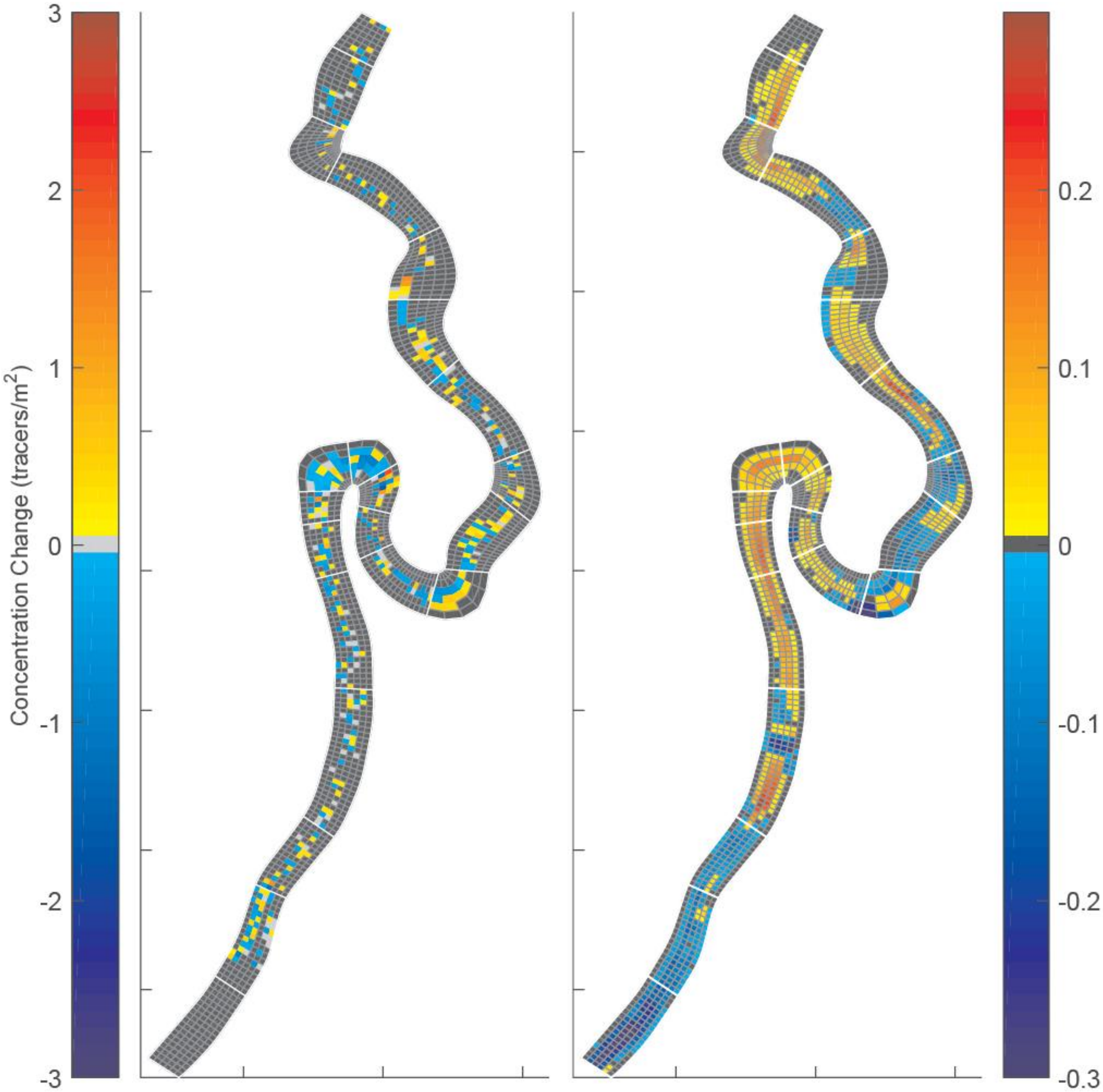

Figure 33. Maps of the 2011 tracer concentration change (left) and model bed elevation change (right). The clearest patterns of tracer concentration change are erosion on the first meander and a narrow band of deposition on the second meander. The model predicts deposition around the both the first and second meander bend.

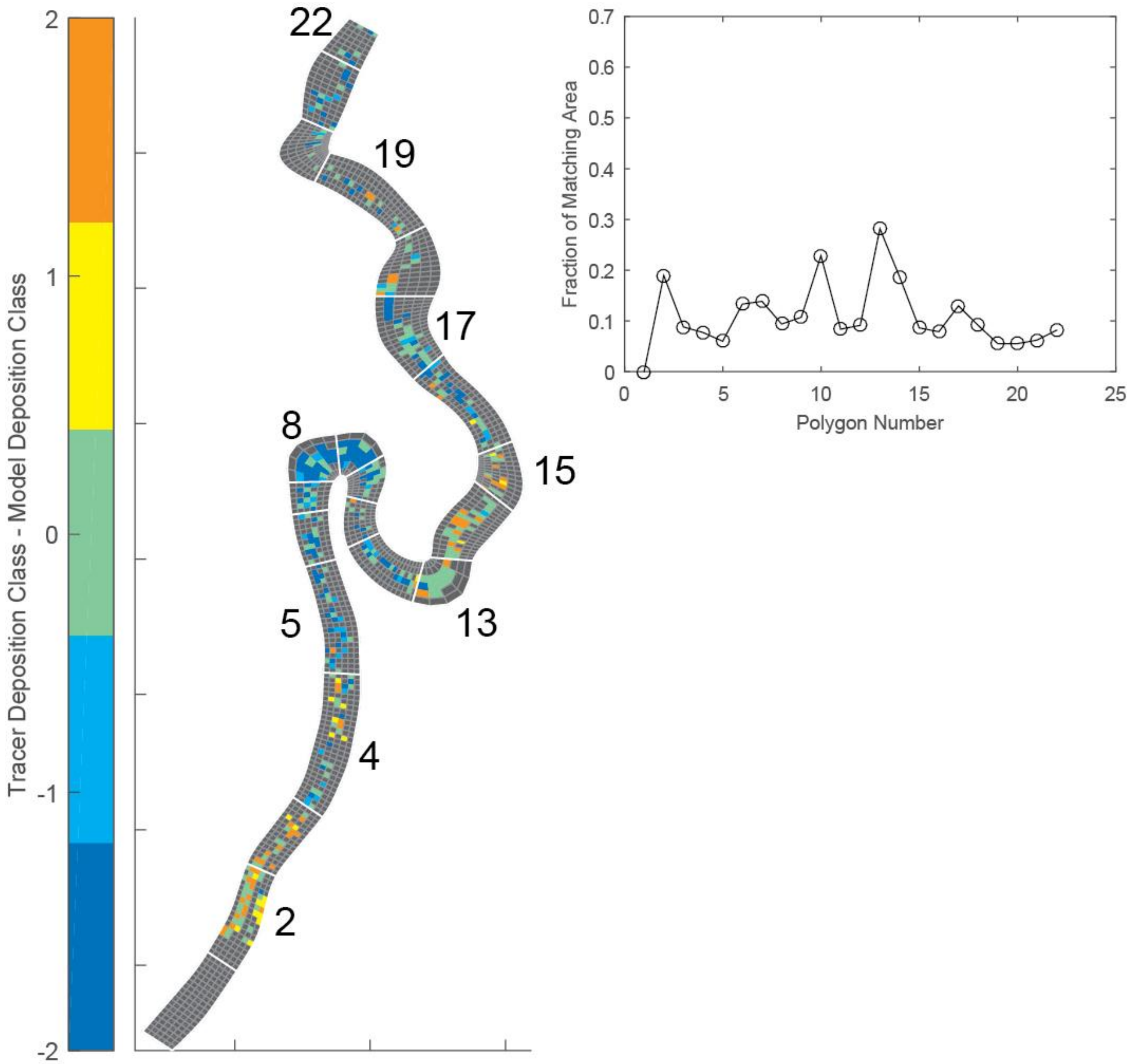

Figure 34. Map showing the 2011 erosion or deposition similarity index. The graph shows the fraction of matching area in each polygon. The areas of strongest agreement are areas of deposition in polygons 10 and 13.

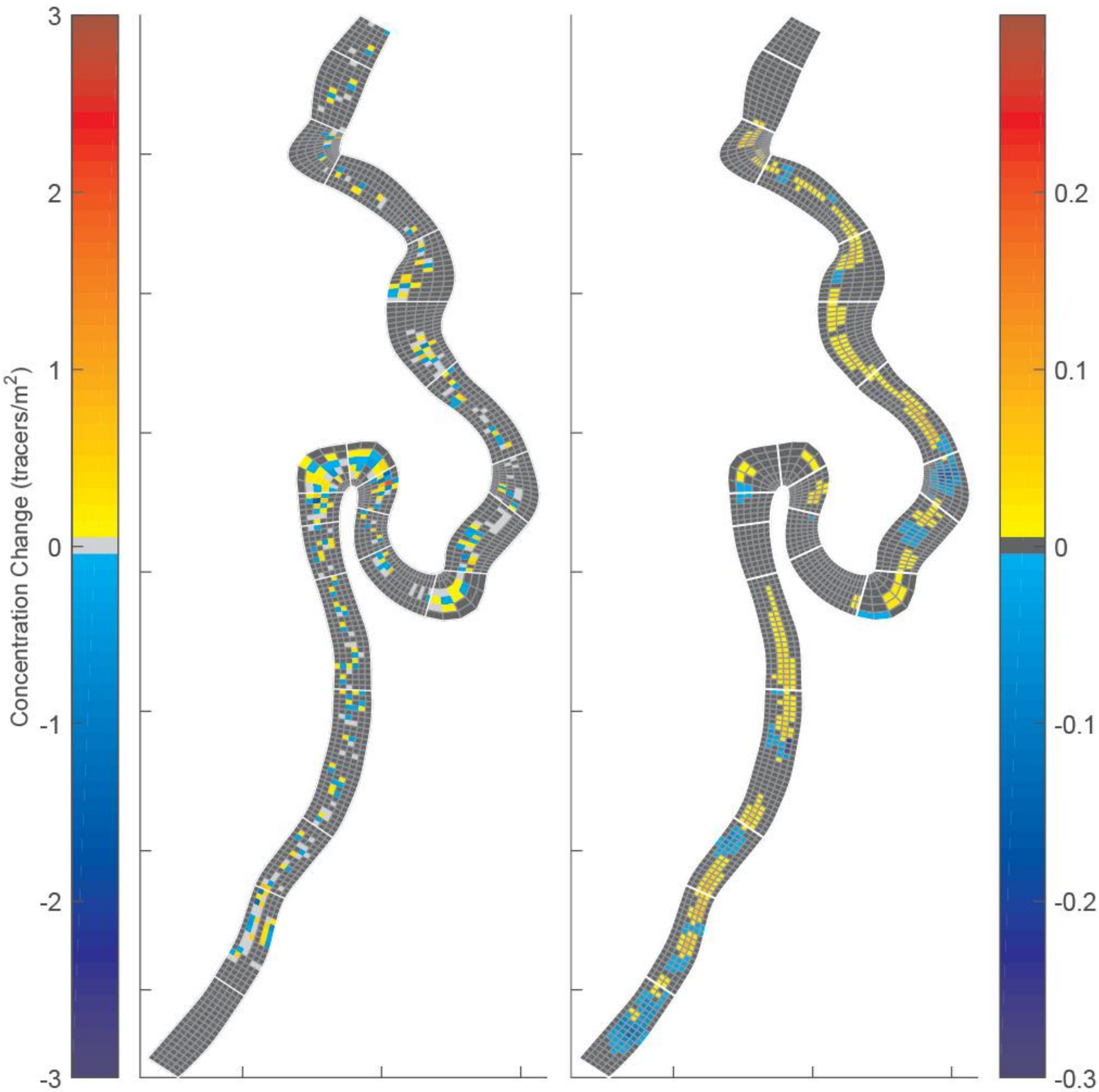

Figure 35. Maps of the 2012 tracer concentration change (left) and model bed elevation change (right). 2012 did not exceed the transport discharge threshold, but there were small amounts of tracer movement around the first and second meanders. The model also predicted very little topographic change.

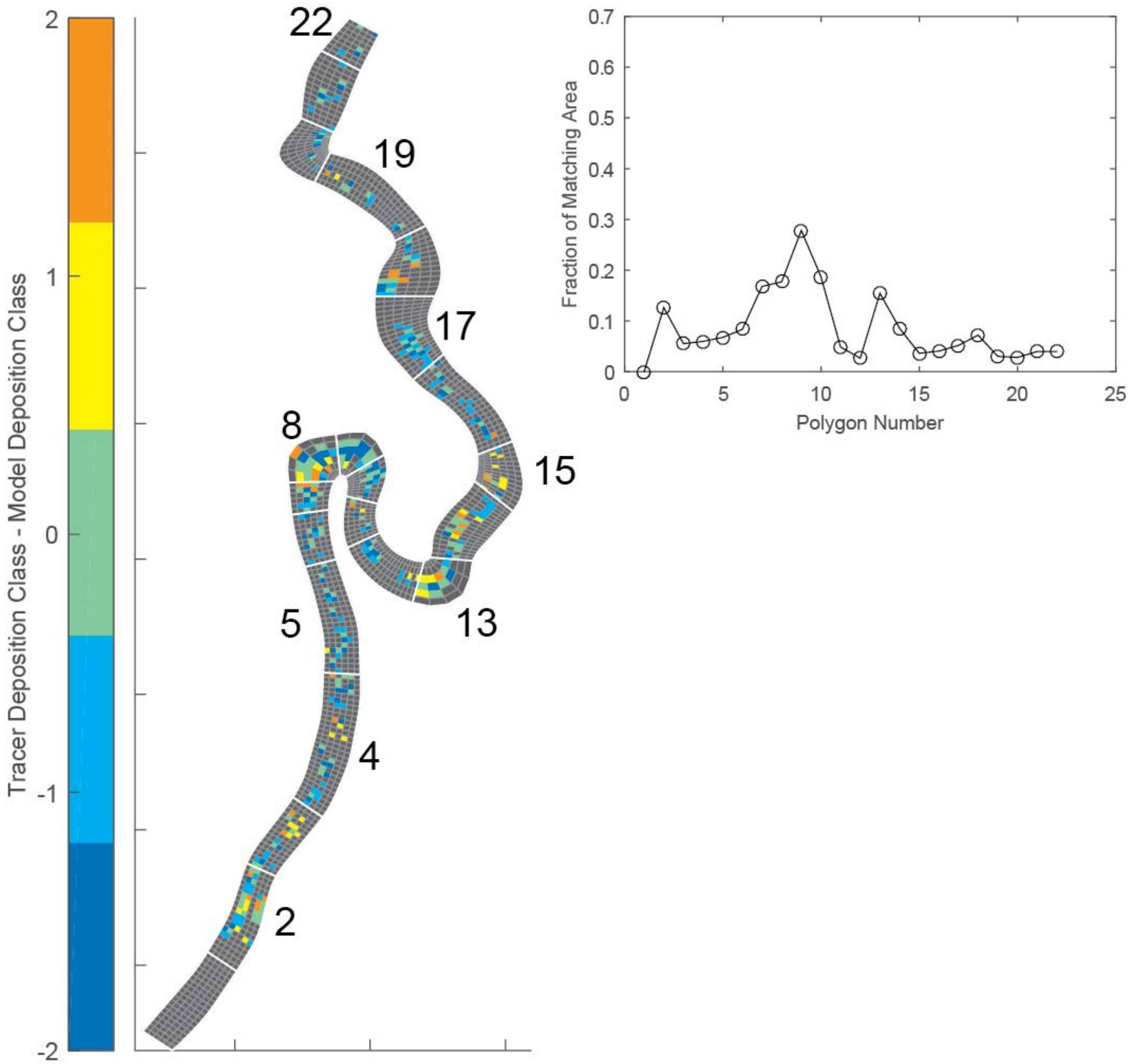

Figure 36. Map showing the 2012 erosion or deposition similarity index. The graph shows the fraction of matching area in each polygon. There is little similarity other than small amounts of tracer accumulation (and model deposition) in polygons 9 and 13.

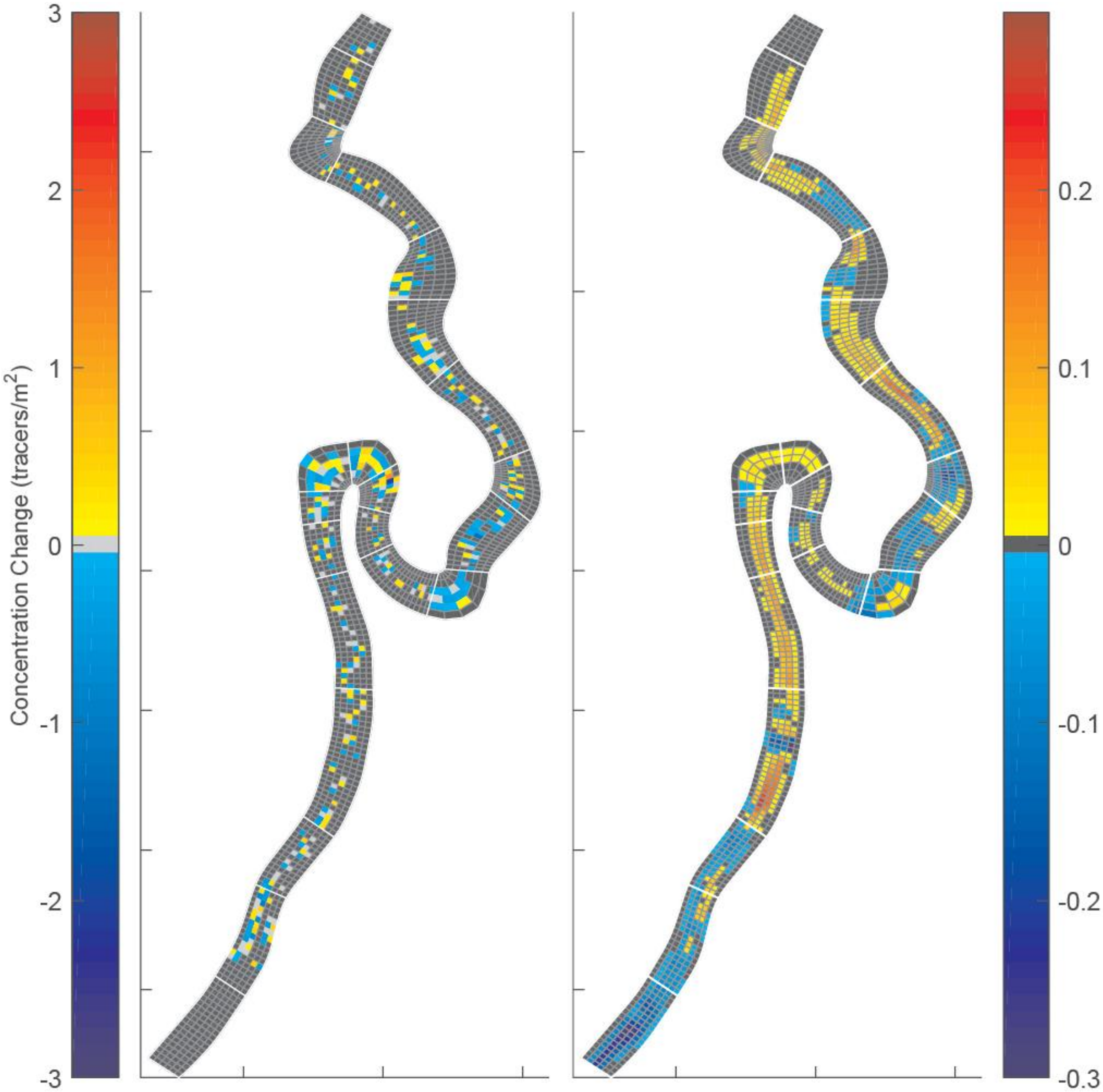

Figure 37. Maps of the 2013 tracer concentration change (left) and model bed elevation change (right). Tracers accumulated in some parts of the first meander and the model showed consistent topographic change. The second meander bend lost tracers and the model showed a somewhat consistent pattern.

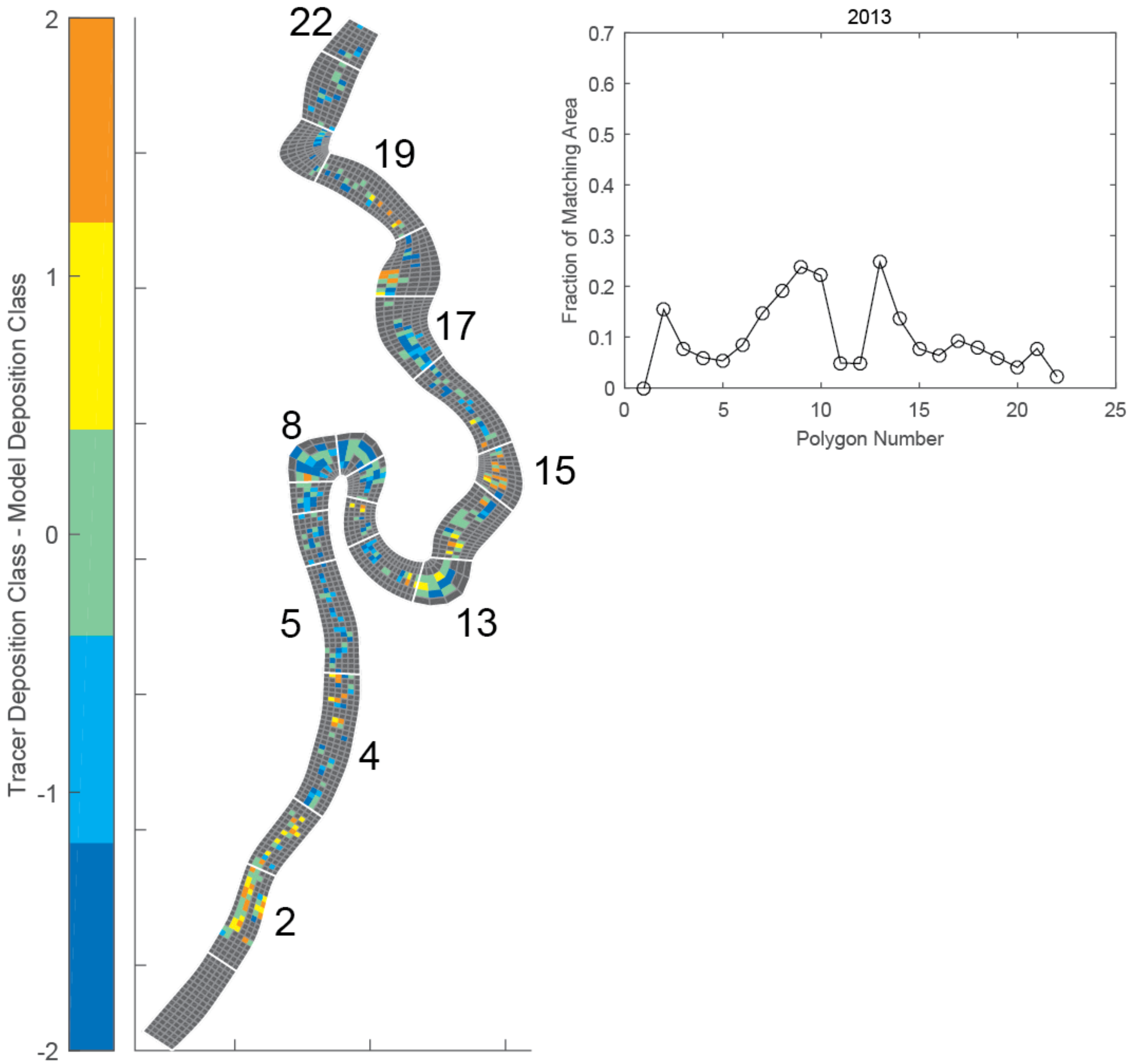

Figure 38. Map showing the 2013 erosion or deposition similarity index. The graph shows the fraction of matching area in each polygon. There is agreement in an area of deposition in polygons 9 and 10 and agreement in an area of (mostly) erosion in polygon 13.

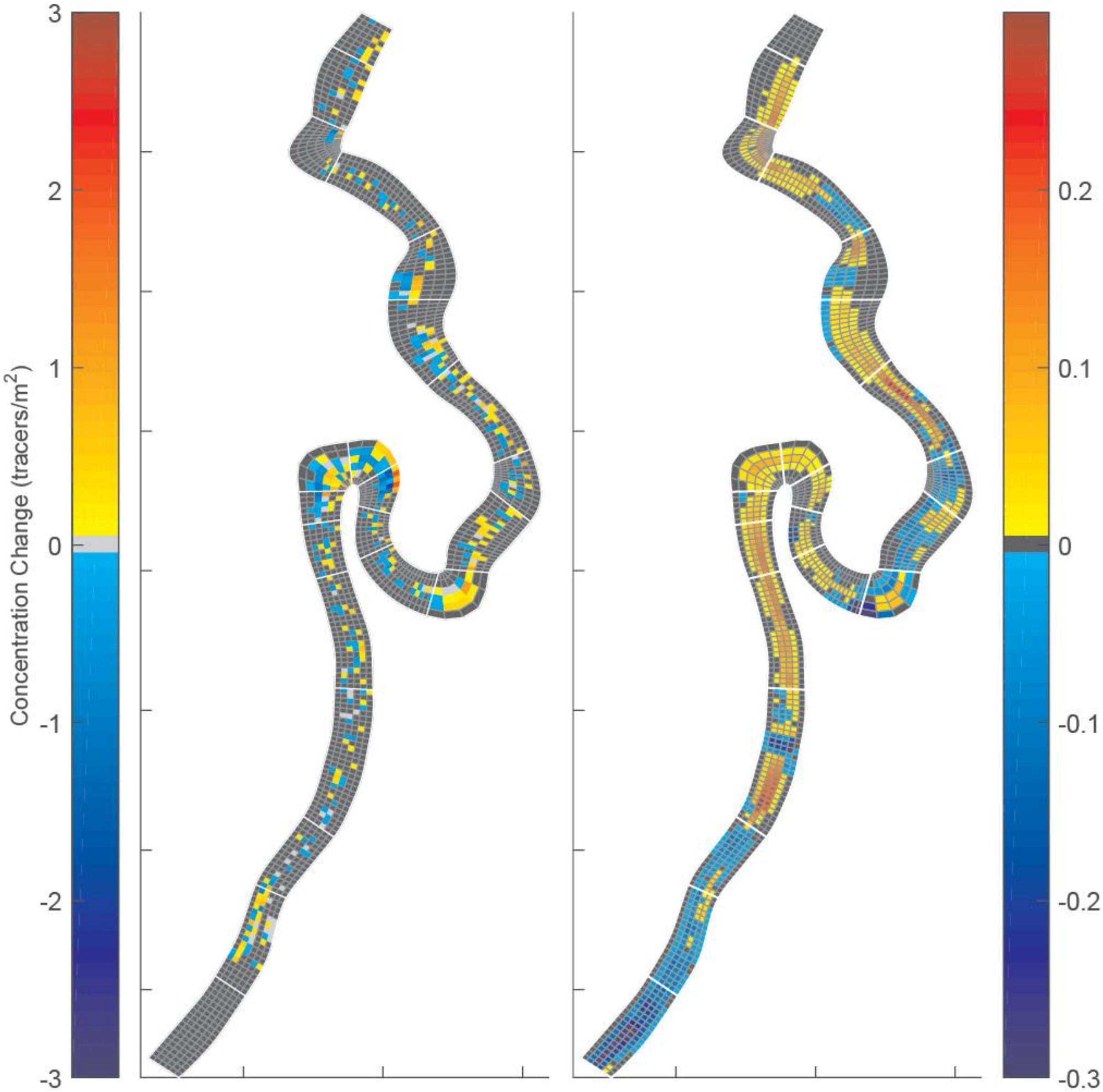

Figure 39. Maps of the 2014 tracer concentration change (left) and model bed elevation change (right). Tracers concentrated along the downstream end of the first meander and at the apex of the second meander. The model predicted mostly deposition around the first meander and a mix of erosion and deposition around the second meander.

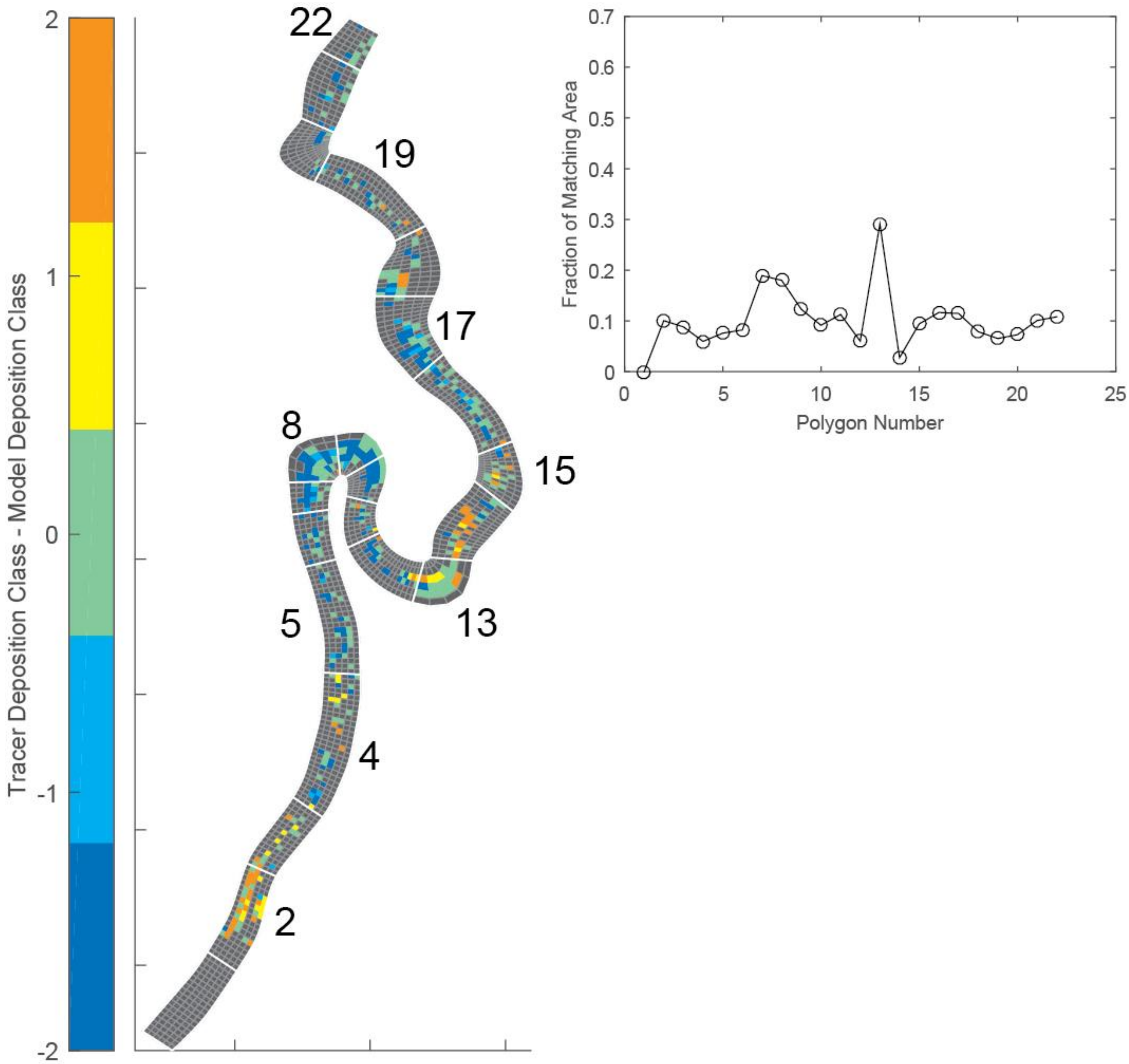

Figure 40. Map showing the 2014 erosion or deposition similarity index. The graph shows the fraction of matching area in each polygon. Deposition in polygon 13 is the strongest area of agreement.

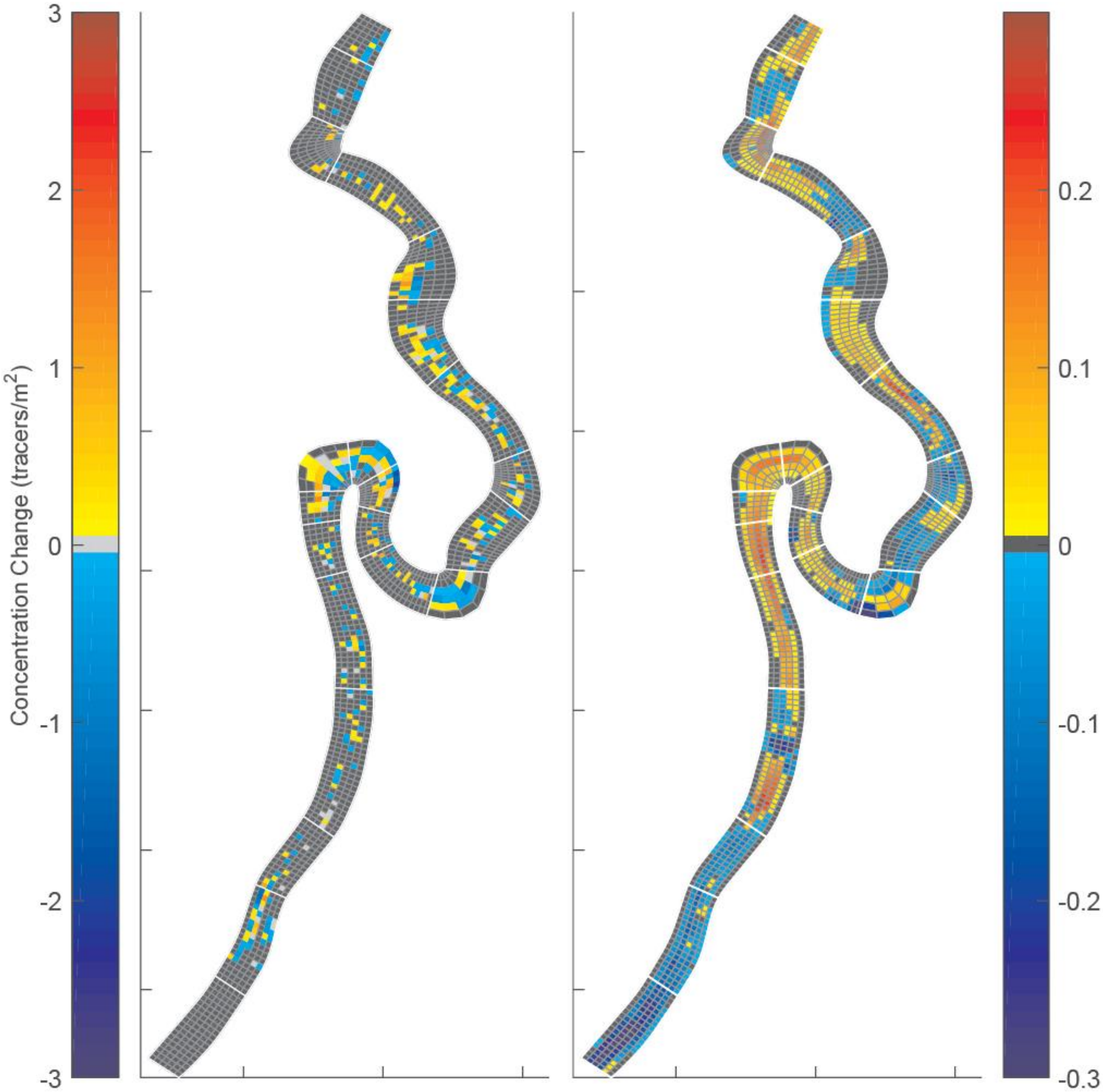

Figure 41. 2015 tracer concentration change (left) and model bed elevation change (right). The model pattern of topographic change is similar to other high flow years. The tracer concentration map is showing the effects of the depletion of the upstream tracer supply.

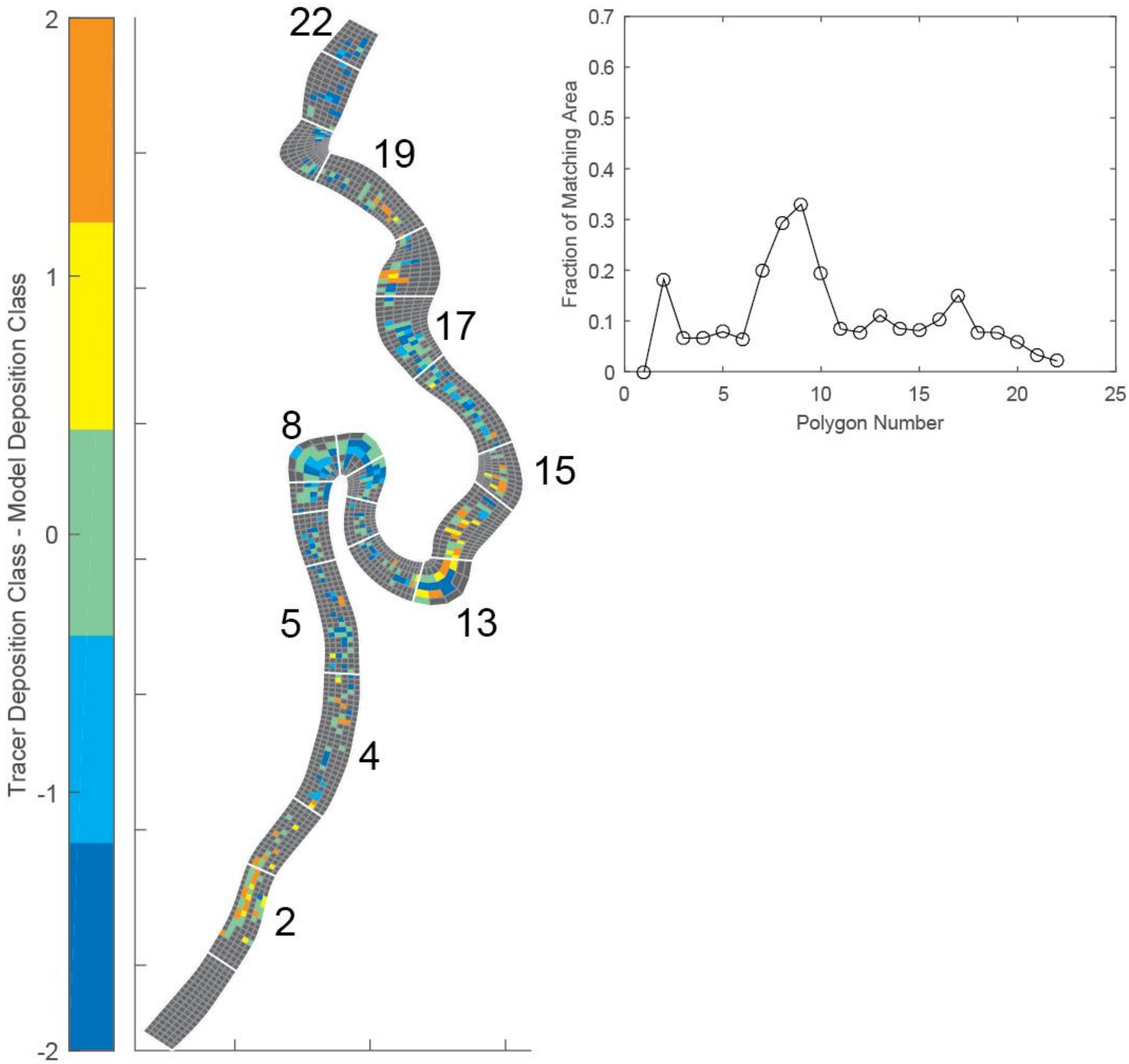

Figure 42. Map showing the 2015 erosion or deposition similarity index. The graph shows the fraction of matching area in each polygon. There is minor agreement in the areas of deposition around the first meander bend (polygons 9 and 10) and further downstream on a gravel bar in polygon 17.

Conclusions

As configured for this study, SRH-2D does not conserve sediment mass, which casts doubt on all further conclusions. The amount of sediment leaving the model is greater than the sum of inlet sediment and sediment sourced from the model streambed. Detailed analysis of the divergence of flux across successive monitoring lines showed that the majority of excess sediment flux is being "created" in just a few areas of the model and the behavior is mostly consistent from year to year. This suggests that the cause of the violation of sediment mass conservation is related to the model mesh and/or the model streambed topography. More research into this issue is warranted. It is possible that the sudden spikes in the sediment flux are related to the excess mass.

In spite of the violation of sediment mass conservation, there is correspondence between average model sediment flux and average tracer transport distance, both in the pattern (Figure 21) and the specific values of sediment flux that are predicted by equations that link the Lagrangian tracer transport statistics to the Eulerian model sediment fluxes (Figure 23). The model flux scales linearly with cumulative excess energy, consistent with the scaling of mean tracer displacement, and the flux is predicted by the tracer statistics to within a factor of two.

The correspondence between yearly tracer concentration change and the model topographic change is not as strong. The model is broadly consistent with the tracer results in that it predicts deposition on gravel bars and erosion in the stream segments between bars. However, the model likely over-predicts the amount of deposition. Running the flood sequence as a single model run or using the topography from a previous run as the initial condition for the next might improve the results if the model reached a topographic quasi-equilibrium. The comparison is further hampered because the upstream tracer supply changes as tracers are distributed along the study reach. This makes it difficult to interpret how patterns of tracer concentration change relate to changes in channel morphology. A final complication relates to the choice of spatial scale at which to compare the model to the tracer data. The comparison becomes "noisy" at high spatial resolution, but important details may be lost if the areas compared are larger than the scale of the channel bed morphology.

In summary, the success of SRH-2D at predicting average tracer travel distance is surprising and suggests that SRH-2D could be useful in designing and analyzing gravel augmentation programs, as has been shown by previously by *Gaeuman* [2014]. Further research into conservation of sediment mass, the origin of sudden spikes in transport rates, and the development of a method to predict individual tracer trajectories would improve the utility of SRH-2D as a sediment transport model.

References

Allan, J. C., R. Hart, and J. V. Tranquili (2006), The use of Passive Integrated Transponder (PIT) tags to trace cobble transport in a mixed sand-and-gravel beach on the high-energy Oregon coast, USA, *Marine Geology*, *232*(1-2), 63-86.

Bagnold, R. A. (1977), Bed load transport by natural rivers, *Water Resour. Res.*, *13*(2), 303-312.

Bradley, D. N. (In Review), Direct observation of heavy-tailed storage times of bedload tracer particles causing anomalous super-diffusion, *Geophys. Res. Lett*.

Bradley, D. N., and G. E. Tucker (2012), Measuring gravel transport and dispersion in a mountain river using passive radio tracers, *Earth Surface Processes and Landforms*, *37*(10), 1034-1045.

Bradley, D. N., G. E. Tucker, and D. A. Benson (2010), Fractional dispersion in a sand bed river, *J. Geophys. Res.*, *115*, 33-52.

Clifford, N. (1993), Differential bed sedimentology and the maintenance of riffle-pool sequences, *Catena*, *20*(5), 447-468.

DeVries, P. (2002), Bedload layer thickness and disturbance depth in gravel bed streams, *Journal of Hydraulic Engineering*, *128*(11), 983-991.

Ergenzinger, P., and K. Schmidt (1990), Stochastic elements of bed load transport in a step-pool mountain river, paper presented at Hydrology in Mountainous Regions II, Artificial reservoirs, water and slopes. Publication 194. IAHS, Wallingford, Oxfordshire, UK, .

Ferguson, R., and S. Wathen (1998), Tracer-pebble movement along a concave river profile: Virtual velocity in relation to grain size and shear stress, *Water Resour. Res.*, *34*(8), 2031-2038.

Ferguson, R., D. Bloomer, T. Hoey, and A. Werritty (2002), Mobility of river tracer pebbles over different timescales, *Water Resour. Res.*, *38*(5), 1045.

Gaeuman, D. (2014), HIGH-FLOW GRAVEL INJECTION FOR CONSTRUCTING DESIGNED IN-CHANNEL FEATURES, *River Research and Applications*, *30*(6), 685-706.

García, M. (2008), Sediment Transport and Morphodynamics, in *Sedimentation Engineering*, edited, pp. 21-163.

Goodwin, K. L., J. P. Johnson, and D. N. Bradley (In preparation), Changing bedload transport rates in a snowmelt-fed mountain stream quantified by motion sensor-embedded tracers: Bedload transport hysteresis, anomalous diffusion, and changing threshold of motion across timescales, *in preparation*.

Greimann, B., Y. Lai, and J. Huang (2008), Two-Dimensional Total Sediment Load Model Equations, *Journal of Hydraulic Engineering*, *134*(8), 1142-1146.

Haschenburger, J. (2011b), The rate of fluvial gravel dispersion, *Geophysical Research Letters*, *38*(24).

Haschenburger, J. K. (2011a), Vertical mixing of gravel over a long flood series, *Earth Surface Processes and Landforms*, *36*(8), 1044-1058.

Haschenburger, J. K., and M. Church (1998), Bed material transport estimated from the virtual velocity of sediment, *Earth Surface Processes and Landforms*, *23*(9), 791-808.

Hassan, M. A., and D. N. Bradley (2017), Geomorphic Controls on Tracer Particle Dispersion in Gravel-Bed Rivers, *Gravel-Bed Rivers: Process and Disasters*, 159.

Hassan, M. A., M. Church, and A. P. Schick (1991), Distance of movement of coarse particles in gravel bed streams, *Water Resour. Res.*, *27*(4), 503-511.

Lai, Y. (2010), Two-Dimensional Depth-Averaged Flow Modeling with an Unstructured Hybrid Mesh, *Journal of Hydraulic Engineering*, *136*(1), 12-23.

Lamarre, H., and A. G. Roy (2008), A field experiment on the development of sedimentary structures in a gravel-bed river, *Earth Surface Processes and Landforms*, *33*(7), 1064-1081.

Lamarre, H., B. MacVicar, and A. Roy (2005), Using passive integrated transponder (PIT) tags to investigate sediment transport in gravel-bed rivers, *Journal of Sedimentary Research*, *75*(4), 736-741.

Laronne, J., and M. Carson (1976), Interrelationships between bed morphology and bed-material transport for a small, gravel-bed channel, *Sedimentology*, *23*(1), 67-85.

Legleiter, C. J., and P. C. Kyriakidis (2006), Forward and inverse transformations between Cartesian and channel-fitted coordinate systems for meandering rivers, *Mathematical geology*, *38*(8), 927-958.

Liébault, F., H. Bellot, M. Chapuis, S. Klotz, and M. Deschâtres (2012), Bedload tracing in a high-sediment-load mountain stream, *Earth Surface Processes and Landforms*, *37*(4), 385-399.

López, R., and J. Barragán (2008), Equivalent Roughness of Gravel-Bed Rivers, *Journal of Hydraulic Engineering*, *134*(6), 847-851.

Milan, D., G. Heritage, and A. Large (2002), Tracer pebble entrainment and deposition loci: influence of flow character and implications for riffle-pool maintenance, *Geological Society, London, Special Publications*, *191*(1), 133-148.

Mueller, E. R., and J. Pitlick (2005), Morphologically based model of bed load transport capacity in a headwater stream, *J. Geophys. Res.*, *110*(F2).

Mueller, E. R., J. Pitlick, and J. M. Nelson (2005), Variation in the reference Shields stress for bed load transport in gravel-bed streams and rivers, *Water Resour. Res.*, *41*(4), W04006.

Nichols, M. (2004), A radio frequency identification system for monitoring coarse sediment particle displacement, *Applied Engineering in Agriculture*, *20*(6), 783- 787.

Olinde, L., and J. P. Johnson (2015), Using RFID and accelerometer-embedded tracers to measure probabilities of bed load transport, step lengths, and rest times in a mountain stream, *Water Resour. Res.*, *51*(9), 7572-7589.

ONSET (2017), HOBO® U20L Water Level Logger (U20L-0x) Manual edited.

Phillips, C. B., and D. J. Jerolmack (2014), Dynamics and mechanics of bed-load tracer particles, *Earth Surf. Dynam.*, *2*(2), 513-530.

Phillips, C. B., R. L. Martin, and D. J. Jerolmack (2013), Impulse framework for unsteady flows reveals superdiffusive bed load transport, *Geophysical Research Letters*, *40*(7), 1328-1333.

Schmidt, K.-H., and P. Ergenzinger (1992), Bedload entrainment, travel lengths, step lengths, rest periods—studied with passive (iron, magnetic) and active (radio) tracer techniques, *Earth Surface Processes and Landforms*, *17*(2), 147-165.

Schneider, J. M., R. Hegglin, S. Meier, J. Turowski, M. Nitsche, and D. Rickenmann (2010), Studying sediment transport in mountain rivers by mobile and stationary RFID antennas, Bundesanstalt für Wasserbau: Braunschweig, Germany.

Seminara, G., L. Solari, and G. Parker (2002), Bed load at low Shields stress on arbitrarily sloping beds: Failure of the Bagnold hypothesis, *Water Resour. Res.*, *38*(11), 31-31-31-16.

U.S. Geological Survey (2013), National Water Information System data available on the World Wide Web (Water Data for the Nation), edited.

Wilcock, P. R., and B. W. McArdell (1997), Partial transport of a sand/gravel sediment, *Water Resour. Res.*, *33*(1), 235-245.

Wilcock, P. R., and J. C. Crowe (2003), Surface-based transport model for mixed-size sediment, *Journal of Hydraulic Engineering*, *129*(2), 120-128.

Wilcock, P. R., A. F. Barta, C. C. Shea, G. M. Kondolf, W. Matthews, and J. Pitlick (1996), Observations of flow and sediment entrainment on a large gravel-bed river, *Water Resour. Res.*, *32*(9), 2897-2909.